THE ENVELOPES OF ERROR, RELIABILITY AND STABILITY OF NASOMAXILLARY LANDMARKS TO ISOLATE TREATMENT EFFECTS IN 3-DIMENSIONS

By

Andrea A. Font Rytzner, D.D.S.

Submitted in partial fulfillment of the requirements for the degree of Master of Science in Dentistry

Thesis Advisor: Manish Valiathan, D.D.S., M.S.

Committee Members: Mark Hans, D.D.S., M.S.D.

Juan Martin Palomo, D.D.S., M.S.D.

Sena Narendran, B.D.S., D.D.P.H., M.Sc.

Department of Orthodontics

School of Dental Medicine

CASE WESTERN RESERVE UNIVERSITY

January 2014

TABLE OF CONTENTS

DEDICATION ..... **II**

ACKNOWLEDGEMENTS ..... **III**

ABSTRACT ..... **IV**

REVIEW OF THE LITERATUR **1**

LITERATURE REVIEW REFERERENCES **33**

STATEMENT OF THE THESIS **38**

MANUSCRIPT FOR PUBLICATION **39**

MANUSCRIPT REFERENCES **62**

APPENDICES **67**

A. IRB approval from CWRU/ Informed Consent 67

B. List of Tables 70

C. Figures representing landmark location: 78

D. Figures representing orientation method: 85

E. Envelope of Error Scattergrams (T1 and T2): 87

F. Reliability Scattergrams: 92

G. RAW DATA 97

Dedication

This thesis is dedicated to my family. My mother, for unconditionally supporting me every step of the way. My father, who taught me to always aim higher. My sister, for her encouragement throughout my journey and my brother, for making my dreams possible.

Acknowledgements

I would like to thank my thesis advisor, Dr. Manish Valiathan, for guiding me though this hard working journey of writing a thesis manuscript and your precious advise inside and outside the field of orthodontics.

Thank you Dr. Martin Palomo for accepting me in this program and for making these years an unforgettable experience in the department. Thank you for your guidance.

Thank you Dr. Mark Hans for the opportunity of attending Case Western Reserve University and for providing the tools to succeed as a specialist.

Thank you Dr. Sena Narendran for your endless help in statistics and for always being available.

Finally, thank you to all the Faculty members of the Orthodontic Department at Case Western Reserve University. You are the core of this program and I will be forever grateful for your time and experience shared.

The Envelopes of Error, Reliability and Stability of Nasomaxillary Landmarks to Isolate Treatment Effects in 3-Dimensions

Abstract

By

ANDREA A. FONT RYTZNER, D. D. S.

OBJECTIVE: to describe the envelope of error, reliability and relative stability of landmarks in the nasomaxillary complex that may be used to isolate treatment effects in 3-D.

METHODS: Existing pre (T_1) and post (T_2) treatment CBCT volumes of 30 randomly selected adolescent patients' were oriented using cranial nerve canals to establish the 3 reference planes. Using a coordinate system, 10 landmarks were identified and the envelopes of error were plotted using scatter graphs. Reliability of all landmarks was assessed with ICC and scatter graphs. The IO, NPF, GPF landmarks were used to evaluate their relative stability and utility in isolating treatment effects.

RESULTS: The variation of the IO, LD and NPF were greater along the axial axis. The axial plane was the least reliable in all landmarks. There was no clear change of direction for most landmarks. The transverse dimension of the IO significantly increased with time. The vertical dimension increased the most variable from T_1 to T_2, especially for IO-GPF. The interdistances of IO, GPF and NPF for the most part was statistical significant.

CONCLUSION: Landmarks had characteristic envelopes of error in all three planes. Tested landmarks were reliable; the least reliable was the axial axis. GPF and NPF were relatively stable areas for future voxel-based superimpositions. Basion might not be a stable landmark over time.

Keywords: Envelope of error, Reliability, Coordinate, CBCT, Maxillary superimposition

Review of the Literature:

The use of three dimensional (3-D) scans was introduced in 1998 in Europe and in 2001 in the United States. Since then, a revolution in the diagnosis and research in dentistry has taken place. Cone beam computed tomography (CBCT) offers images of undistorted dentition and other maxillofacial structures that are used to visualize previously undetectable images in two-dimension (2-D) radiology. Since the use of CBCT in orthodontics, measurements, data collection, and studies have been conducted in an effort to answer questions that could not have been answered before. As a result, a new series of standards and outcomes evaluation methods are currently being explored by researchers around the globe.

Measurements from CBCT images have shown to be accurate in regards to the anatomic structures measured for orthodontic purposes (Baumgaertel, 2009)[1]. Facial growth and development, as well as the ability to assess outcomes are critical in orthodontics.

Rickets[2] stated that one of the applications of cephalometrics is to record and to measure changes. Superimpositions, employing lateral cephalograms have

been traditionally used to describe spatial changes of the craniofacial structures. Using areas of greatest anatomic stability, skeletal as well as dental changes that occur as a result of orthodontic therapy and normal growth can be assessed. There are weaknesses in 2-D imaging because of inevitable loss of information when applied to represent lifelike three-dimension (3-D) structures (Hans, 2001)[3]. Three-dimension structures are projected on a 2-D radiographic film, creating optical illusions of craniofacial anatomy. The mandibular symphysis, the pterygoid fossa, and the "key ridge" are examples of artifacts in cephalometrics that are commonly referred to as anatomical landmarks. Bilateral anatomical structures project a double image in a 2-D cephalogram because the x-ray beam diverges as it passes through the head. The averaging of bilateral structures creates two problems: 1) the fact that the average line is an abstraction based on the anatomy of the patient, and 2) the fact that the averaging also results in a loss of parasagittal information and any true asymmetry of the patient is lost.

Other factors that are additional limitations of cephalometrics are magnification and distortion errors.

The x-ray beams are not parallel to all points of the desired object, thereby creating a magnification that if applied to a bilateral structure, will create unequal magnifications between different planes resulting in distortion[4].

Baumrind and Frantz[5, 6] classified three major error gropus: errors of projection, errors of identification and mechanical errors of measurements. Their work was based on 2-D cephalograms, but may still apply to newer modalities of imaging. Errors of projection were early described in 2-D imaging. The rays which produce a 2-D shadow of a 3-D object are nonparallel and originate from a small source; therefore head films are always distorted enlargements. The enlargement factor varies depending on what plane the estimated point of interest lies.

Errors of identification are involved when identifying specific anatomic landmarks on head films and they were the first to quantify the precision of different landmarks used in standard cephalometric analyses. They aimed a quantification or error in landmark identification and assessing the effect of these errors when using angular and linear measurements. They based their studies on a sample of twenty randomly

selected head films and were traced by each of the five members of a postgraduate class. Sixteen standard cephalometric landmarks were traced, as well as four fiducial points. The data for the study were 100 acetate tracings, five for each of the twenty head films; therefore there were 100 estimates for each landmark. The X and Y values for each landmark were averaged and 16 scattergrams were created, one for each landmark (one point in each scattergram from each tracing). Measurements where the total X + Y error exceeded 1mm were rejected. The average tracings were 0.7mm with a standard deviation around 0.3mm. Then a representative head film was created with a set of 16 "hundred-point scattergrams", each representing the dispersion of estimation for a single landmark around the best estimation for that landmark (the mean of each group of landmarks was considered the best estimate of that particular landmark and was defined by lying in the scattergram origin) and oriented to the sella-nasion line(S-N) [5]. This set the Gold Standard for analyzing reliability in landmark identification for future studies.

Superimposition errors were larger than landmark identification errors. Differences in reliability of estimation were higher among gonion and lower incisal apex. These seemed to be the least reliable landmarks.

Angular and linear measurements will have errors previously introduced by identification error. The absolute values of errors and variability tended to be greater for angular measurements than for linear measurements[6]. For the same reason that reliabilities differed depending on the landmark, angular and linear measurements were not equally reliable. There seemed to be a larger error when the linear measurements were smaller, and when the angular measurements were closer together.

The conclusions of Baumrind's studies[5, 6] were critical. Landmark identification errors are too great to be ignored, the magnitude of error varies greatly depending on the landmark and the distribution of errors was not random, but systematic. Meaning that depending on the landmark, each one has a characteristic and usually noncircular envelope of error. Landmarks that were sharp (lower or upper incisal edge for example) had better

estimates than those that were represented within a gradual curve (gonion, point A or point B for example).

Errors in these types of landmarks seemed proportionately larger and tended to be along the surface where the landmark would be located. Specific mention was made to the prior experience of the judges (the more experience operator, the more reliable one would tend to be), and the importance of a rigorous definition of the landmark for more precision. Sella and nasion are landmarks that should need further explanation, since they are frequently used in cephalometrics for the reference line S-N. The fact that Sella involves a visual estimation of the center of a structure reduced the dispersion, since a visual estimation of a midpoint is a mental averaging process. The gross outliers seen in Nasion were explained by the result of identification errors of different structures. The suggestion that a routine use of replicated measurements was also made, making this an unrealistic goal in clinical practice.

Lagravère et al[4] also concluded that landmarks located on flat or curved surfaces were harder to recognize as a specific reference landmark when using formatted 3-D CBCT images, such as gonion, condylion and

porion. This study also compared the intraexaminer and interexaminer reliability between digital traced cephalograms and those reproduced from CBCT scans. Reliability was measured with the reliability correlation coefficients and even though both reliabilities were greater than 0.9, the means of landmark locations were within 1mm difference when comparing the groups, but slightly higher than 1mm in the CBCT group. The mean measurement errors in landmark identified in CBCT varied from 0.1 to 4mm in all 3 axes. Some landmarks were more variable in a particular axis, but had lower variability in another axes. This was due to the incorporation of the third dimension in the CBCT group, adding potentially greater variation to the measurements. Lagravère et al[4] also made reference to the fact that some landmarks were located in an area with low density therefore making it a harder landmark to identify than those in 2-D cephalograms, such as anterior nasal spine (ANS), posterior nasal spine (PNS) and lower incisor apex. Perhaps the interobserver and intraobserver reliability should have been analyzed with scatter graphs rather than reliability coefficient, since the reliability measured this way will probably always give a high value. A

follow-up on Baumrind's work[5, 6] would have been of use to establish landmark error and distribution in the way of scattergraphs.

A more recent study by Mu-Hsiung Chen et al[7] analyzed the intraobserver reliability in a similar study, comparing CBCT synthesized 2-D cephalograms versus conventional cephalometric radiography. This study recorded the differences in the axes of each landmark as identification errors. Identification errors of both groups were compared using the paired Student t-test. Scatter plots were used to demonstrate the distribution of intraobserver errors in landmark identification. The errors of landmark identification reported in their study ranged from 0.18-1.67mm being clinically acceptable in both groups. They also reported that CBCT 2-D cephalograms had higher identification reliability in some landmarks such as pogonion, gonion and menton.

Intra- and interobserver reliability in 3-D cephalometric landmark identification was also analyzed by de Oliveira et al[8] in 2008. Twelve randomly selected presurgical patients and thirty landmarks were identified by three observers at three independent times. A protocol needed to be established to calibrate the observers prior

to landmark placement. Reliability was calculated with ICC for each coordinate of each landmark. Intraobserver reliability was over 0.9 for 85.55% of the measurements, with the greater frequency in the Z coordinate. The interobserver reliability was over 0.9 for only 65.55% of the measurements. The greater frequency was also in the Z coordinate; perhaps because traditional orthodontic training in lateral cephalograms has educated the operator on how to locate landmarks in the antero-posterior direction, therefore the clinician has more training when locating landmarks in this plane. There was poor reliability on at least two cases in the Y coordinate. Perhaps this is due to lack proper definitions for landmarks in all three planes of space. Considering that the data was collected three times, this was enough to create scatter graphs; additional information about landmark identification should have been given consideration in this study.

In cephalometrics, there is an obvious interest in linear and angular measurements. Many studies have been conducted to analyze these types of measurements. A study conducted in Europe on 3-D sheep fetal cephalometry[9] compared 3-D scan reconstructions and measurements on dry

skulls. Papadopoulos described that the evaluation of direct anthropometric analysis (measuring directly on the skulls) had significant differences between initial and repeated measurements in 7 out of the 56 linear measurements. On the other hand, the 3-D analysis revealed that none of the 56 linear measurements differed significantly. This study also compared cephalometric analysis. When comparing the direct cephalometric analysis versus the 3-D analysis, there seemed to be 5 measurements out of 56 that had an increased difference. This might seem to be due to the specific identification of those landmarks (in greater bone surfaces) or to the fact that these bones where the landmarks were placed were not well mineralized, therefore creating difficulty in the landmark registration. A suggestion was made that perhaps for not mineralized bones, a lower threshold should be considered, but that would mean that the bones would appear denser. They stated that bone growth evaluation could be performed with cephalometric 3-D analysis as an accurate and reliable way.

Brown et al.[10] also analyzed linear measurements. They compared in vitro reliability and accuracy of linear measurements between cephalometric landmarks on CBCT

scans with direct measurements on human skulls. Linear dimensions in the vertical, transverse and horizontal planes were represented in the landmarks that were chosen. Some of these landmarks included nasion, ANS, A point, PNS, B point, menton, medio-orbitale (the point on the medial orbital margin that is the most distal point along the frontomaxilary suture), lateral piriform aperture, antegonion, gonion, zygomatic arch and condylion. The reliability of the measurements taken directly from the skulls was greater than those taken from the 3-D renderings. The fact that the mean error of the 3-D measurements was less than 1mm seemed consistent with other reported mean error values. One possible explanation for the fact that the skull measurements had a higher reliability was that the landmark identification in these was only taken once, while the linear measurements were independently taken three times by consensus of two observers. The landmark identification on the 3-D images was repeated three times by a single operator.

Superimpositions have been a way of evaluating and analyzing treatment effects and outcomes. For years this procedure has been analyzed using 2-D cephalometrics. The

immediate problem that this presents is that stable landmarks need to be identified prior to superimposing images. Cephalometrics has also been used for longitudinal facial growth studies[11]. As Sekiguchi mentioned, landmarks selected for individual bone studies, such as the mandible or the maxilla, usually differ from those used for anthropometric values and even orthodontics itself. Landmarks that are usually used in the mandible include pogonion, gonion and condylion. The maxilla, however, represents a more complex problem because of the direction of growth and therefore, more infrequent landmarks have been used for growth studies. These landmarks include the nasomaxilary suture, the infraorbital margin, the anterior nasal spine, prosthion, the zygomaticomaxillary suture, the distal alveolar margin and the pterygomaxillary fissure. Sekiguchi[11] studied how the variability of such landmarks could be minimized and discussed possible problems such landmarks could give in 2-D cephalometrics.

Sekiguchi[11] described some of these variations: the infraorbital margin, also known as orbitale, is one of the most variable landmarks and is more variable in the horizontal dimension than on the vertical dimension. The

anterior nasal spine was of the more variable landmarks, but is found to be accurate vertically. The zygomaticomaxillary suture is equivalent to the key ridge, which is located as a curved image on the zygomaxillary process of the maxilla. In 2-D this is a difficult landmark to locate, because of the fact that images overlap and roots of teeth are in the way as well as the lower wall of the maxillary sinus. This is an area that cannot be represented in a 3-D image, as the key ridge is a result of the superimposition of structures and is only seen on a 2-D cephalogram.

It is imperative to understand the importance of accuracy when speaking about landmark registration. The need of structures being represented accurately is important when superimpositions take place. Superimposition on the cranial base structures has been an extended area of research and different methods differ according to reference structures used within the skull[12]. In 2-D cephalometrics, the cranial base is often used for superimpositions to show both hard-tissue and soft-tissue profile changes because it has minimal changes after neural growth is completed. Most of the cranial base superimpositions on 2-D have been estimated under the

assumption that the anterior cranial base is stable because the brain has finished growing by the age five. However, Enlow and Hans (2008) showed that the floor of the cranium continues to grow and undergo remodeling changes throughout the childhood years; therefore, the cranial base is not truly stable and unchanging. This presents a problem when trying to use reference landmarks in 3-D that have been previously used in 2-D superimpositions because it produces unreliable results. It is necessary to find new stable reference landmarks when using 3-D imaging.

Dentoalveolar changes in response to orthodontic therapy have been estimated from lateral cephalograms with maxillary and mandibular superimpositions. Stable reference landmarks that do not change in time should be used as a reference for superimposition. Studies with implants have showed stable landmarks in time and made it possible to superimpose lateral cephalograms in growing patients. We then have the ability to record changes due to orthodontic mechanisms that are unaided by natural body growth and development. Therefore, if we want to describe true maxillary teeth movement by orthodontic

forces, we must superimpose in the maxilla and let the growth changes be expressed elsewhere.

Julius[13] reviewed the early methods for maxillary superimposition described in the literature. Keith and Campion (1922) used the nasopalatal and oral-palatal surface of the maxilla as registration landmarks. Brodie in 1948 suggested the registration landmarks to be the palatal plane and the pterygomaxillary fissure (PTM), but this was not accurate as the change was explained by the appositional growth of the tuberosity in the maxilla. Brodie mentioned that the development of second molars frequently obscures PNS. Nowadays with CBCT imaging this is a problem that may be overcome. Schaeffer (1949) utilized the use of the palatal plane and either anterior nasal spine (ANS) or posterior nasal spine (PNS) as registration landmarks, since he thought the palatal plane descended parallel during growth.

This has been discredited by Bjork[14] when he demonstrated the rotation of the palatal plane with natural growth with the use of implants in his sample. Steiner (1953) pointed out that when superimposing on the superior and inferior borders of the palate as well as ANS or PNS, it underestimates the eruption of the

dentition by 30% to 50%, and masks the downward remodeling of the maxilla and the palate. In 2-D cephalometrics there is difficulty in tracing some of the structures in the maxilla, such as the superior border of the palate and ANS[13]. He also defined PNS as an unstable area, since it alters during growth. Moore (1959) explained vertical and horizontal growth affected in the maxilla. He noted that the best way to superimpose was on the palatal plane and pterygomaxillary fissure and that the horizontal growth of the tuberosity results in a forward position of ANS. The amount of vertical alveolar growth would manifest itself in the downward movement of the maxillary dentition. Moss and Greenburg (1967) noted a constancy of relationship of the infraorbital canal and foramen after superimposing cephalograms.

Several methods of maxillary superimposition have been described in a more recent literature[15, 16]. Different techniques superimposing on the palatal plane including superimposition registration at pterygomaxillary fissure (PTM), anterior nasal spine (ANS), posterior nasal spine (PNS), internal palatal structures, nasopalatal and oropalatal surfaces as well as anatomically best fit superimposition. It has been clearly stated that

depending on what registrations are used for superimposition, erroneous information concerning patterns of bone growth and remodeling can be obtained, as well as distortion of tooth movements[15-17].

Bjork's work defined a new era in superimpositions. His implant work studies[14, 18] vastly improved our understanding of stable landmarks that may be better employed for superimpositions. Facial development is characterized by a rotation involving both jaws, furthermore a forward rotation of mandible being more than twice the forward rotation of the maxilla[14]. It was shown that the entire increase in the length of the maxilla takes place posteriorly, with little if any remodeling on the anterior surface[19]. Apart from the sutural growth, the development in height takes place by appositional growth of the alveolar process in combination with a resorptive lowering of the nasal floor. In one of Bjork's implant studies[18], the nasal floor was found to remodel according to the direction and magnitude of the rotation of the maxilla showing a great stability irrespective of the direction and magnitude of the rotation. The remodeling was greatest anteriorly or posteriorly according to whether the rotation was,

respectively, forward or backward. Therefore, we can say that the rotation of the maxilla was masked by the remodeling of the nasal floor, which barely changed. These are important factors to consider when considering maxillary growth and need to be taken into account for superimpositions.

Baumrind et al.[20] also studied subjects through the implant method. The goal of his study was to assess cumulative changes on the magnitude and pattern of remodeling of the superior and anterior surfaces of the maxilla, as viewed on the lateral cephalogram. The use of metallic implants in 31 subjects with a cephalogram taken annually for and average period of 9 years were used. Cumulative changes over the years in position of three landmarks were recorded. Point A, ANS and PNS were used as landmarks and the relationship of the displacement of each of these points relative to the superimposition on the maxillary implants was described.

Confirming with Bjork's implant studies[18], Baumrind and coworkers[20] found a high level of confidence in the fact that the superior surface of the maxilla remodels downward during the period of growth ranging from 9-16 years of age. Mean rotation of the ANS-PNS line relative

to the implant was 1.1 degrees in a clockwise rotation of the maxilla, what Baumrind describes as "forward" direction. This rotational change was variable with a standard deviation of 4.6 degrees and a range of 11.3 forward rotation to 6.7 backward rotation meaning that the individual discrepancy is large, but the tendency was the forward movement. This might suggest that not all subjects would manifest a forward rotation of the maxilla, but may or may not have a tendency towards the clockwise rotation. This study also provided strong evidence that the palate elongates anteroposteriorly mainly by the backward remodeling of structures locates posterior to the region in which placed, since there was more displacement at PNS than ANS relative to the implant placement.

A major drawback of this study was that the sample included treated and untreated patients. Even though they incorporated this data in the study, it would have been preferable to have a treated group matched with a non-treated group and assess the differences. Paired t-tests were made between these two subgroups, and some statistical significant changes were reported. It was a relatively small non random sample, so definitive

conclusions should be drawn with caution. There seemed to be statistical significance in both the X and Y planes. These included the horizontal axis in PNS and ANS between the ages of 8.5-14.5 and the vertical axis in PNS and A point between the ages of 8.5-13.5 years of age and 8.5-0.5 years of age respectively.

Julius[13] also described a serial cephalometric study of the metallic implant technique and methods of maxillary and mandibular superimpositions. He mentioned several stable anatomic relationships in the maxilla based on his 21 patient sample. He noted: a parallelism and approximate location of the posterior and key ridge surfaces of the maxillary zygomatic process; a parallel relationship of the outlines of the anterior cranial base and cribiform plate of the ethmoid bone; an anterior and vertical location on the infraorbital foramen and a clockwise rotation and remodeled lowering of the palatal plane approximately three degrees in the anterior region.

Baumrind[21] studied the pattern of maxillary remodeling when different methods are used to superimpose the maxilla. Measurements were made on 31 subjects with metallic implants and quantified the differences in displacement of the implant landmarks in the same sample

using the standard “anatomical best bit”. In this sample, the anatomical best fit superimposition was found to lose important information on the downward remodeling of the superior surface of the maxilla that had been detected when the implant superimposition was used. When the anatomical best fit was used, a small upward displacement of the line ANS-PNS was observed. In the anteroposterior (AP) direction, the tendency toward backward displacement of skeletal landmarks through time that had been detected with the implant superimposition was replaced by a small forward displacement of ANS and Point A together with a reduced backward displacement of PNS. The anatomical best fit superimposition appears to understate the small tendency toward backward remodeling when observed with the implants as well as the downward remodeling of the palate by an average of about 0.3 and 0.4 mm per year, although this value differs at different ages and time points.

Orthodontists nowadays do not routinely use implants as a guidline; therefore clinicians and researchers must necessarily continue to use anatomically based superimpositions similar to that of the anatomical best fit superimposition. Systematic errors will be incurred

if this method is used. Therefore, the necessity of establishing reliable maxillary landmarks seems imperative if CBCT superimposition can be used.

Research has been done to try to identify reference points for 3-D cephalometric analysis. Lagravere[22] proposed the landmark ELSA, a reference point located equidistant to the points in the centers of each foramen spinosum because its location was shown to have a low identification error in the vertical and the horizontal plane as studied by Williamson et al. Intraexaminer reliability was 0.998, and was therefore was concluded to be an adequate landmark in 3-D analysis.

Doppel[23] investigated with implants if there are any stable anatomic landmarks in the maxilla that would be reliable for the maxillary superimposition. Using lateral cephalograms, Doppel found that the internal structure of the palate was of limited value as a stable area of registration but appeared to be the most reliable landmark. The zygomatic process of the maxilla was found to be the most reliable anatomic landmarks when tracing lateral cephalograms of maxillary superimpositions. However, the infraorbital foramen, pterygomaxillary fissure (PTM), anterior nasal spine (ANS), posterior

nasal spine (PNS), A point (A) and the superior and inferior borders of the palate were not stable landmarks. The drawback of this study was that there was no differentiation between the 50 subjects that had been treated with standard edgewise appliances, headgear, class II/III elastics and treated extraction or nonextraction. Therefore these results cannot be precise when trying to identify stable landmarks in the maxilla for the maxillary superimposition.

Houg[24] reviewed Steiner's work on maxillary superimposition. Steiner had described the use of the palate by registering on either ANS or PNS. A cited limitation was the superior surface of the palate that is hard to trace accurately in a 2-D film and the lingual curve of the palate alters during orthodontic treatment, as stated before. He mentioned that ANS varies according to the angulation of the headfilm (something overcome by 3-D imaging). Steiner advocated analyzing the changes by superimposing on a point as close as possible to the area to be assessed in order to rule out growth. Houg also reviewed Bjork's work and noted the increase in maxillary height was revealed when the lowering of the nasal floor exceeded the contribution of growth at the fronto-

maxillary suture. He studied the development of the maxilla in 35 children, with tracings from 8 years to 15 years of age. Each individual had to have at least three headfilms taken at not less than one year interval. Several landmarks were used distributing them in three analyses. The concordance-discordance analysis included spheno-ethmoid plane, the apex of the pterigomaxillary fissure, ANS, A point, anterior area of the palate, anterior and posterior boundry of the zygomatic arch and prosthion. The antero-postero analysis landmarks were the midpoint between the intersection of the great wings of the sphenoid (upon the spheno-ethmoidal plane), apex of the pterigomaxillary fissure, first molar, posterior border of the zygomatic arch, orbitale, A point, prosthion, ANS and central incisor. Finally, for the palatal-occlusal analysis,the palatal and occlusal plane were used. A combination of these analyses was used, based on the inter-comparison of the maxillary areas, evaluating the constancy relationship between each other. The idea was to find constant relationships that would be able to be used in superimposition.

They revealed a uniformly low frequency of constancy in the relationship they had to one another. Changes

varied in a peculiar way to each individual. The alveolar bone has a down and forward pattern of growth when compared to the body of the maxilla being more increased in the molar area than the incisor area in this particular age group and in quantity. Houg[24] found that the internal outline of the anterior area of the palate was a good area for superimposition. The trabecular patters in the anterior area of the maxilla appeared serially stable, therefore being an aid in superimposition. ANS varied as the position of the patient varied with the cephalostat.

It seems that there will always be ongoing debates regarding what landmarks are stable in 2D. The much used sella-nasion (S-N) has received much justified criticism as longitudinal reference in a study by Ghafari[12]. He agreed with Baumrind, Miller and Molthen[25] that when superimposing the cranial base registering at the S-N line versus superimposition on best anatomical fit of the cranial base (structures of the anterior cranial fossa, between the anterior clinoid process and crista galli) rotational errors for the best fit superimposition were relatively smaller. This might have led to other investigators such as Cevidanes[26] to develop a best fit

superimposition based on voxel base registrations, using a large "stable" area as a reference for superimposition. Therefore, the idea that not one landmark or a group of landmarks, but an area around a defined stable point seems indirectly linked to superimposition significance became important.

With the use of 3-D imaging, superimpositions have become an even more complex problem. Identification of stable and reliable landmarks in 3-D may not be assumed based on previously used 2-D landmarks. The incorporation of the transverse dimension creates the additional plane when considering orientation issues.

Bjork's work stated that the mandibular nerve canal during growth remained unchanged[27], establishing the assumption that some cranial nerves remained unchanged after a certain period of time. Lagravère et al.[28] tested the accuracy and reliability of cranial base foremen locations in CBCT. Foramina spinosum, ovale, and rotundum, and the hypoglossal canal all provided high intraexaminer reliability and accuracy, and can be considered acceptable landmarks to use in establishing reference coordinate systems for future 3-dimensional

superimposition analysis. Wu et.al[29] developed a reliable way of orienting the cranial base in three dimensions using the cranial nerves with an underlying assumption that they do not change during growth.

Lagravere[30] et al. also proposed certain landmarks and planes in an attempt to standardize 3-D orientation. Four landmarks were chosen for this standardization. ELSA (midpoint between both foramina spinosum) was located and identified as the 0, 0, 0 coordinate. Location of the superior-lateral border of the external auditory meatus (SLEAM) of the right and left side, and the mid-dorsum of foramen magnum (MDFM) was made. Intrareliability was obtained by replotting these landmarks three times per image and was determined by the intraclass correlation coefficient. The planes were then located using these landmarks. The x-y plane (axial-horizontal plane) was determined by the ELSA and SLEAM (right and left). The z plane (sagittal-vertical plane) was determined perpendicular to the x-y plane and passing through ELSA and MDFM. All the four landmarks were chosen in the middle and posterior cranial base. This area has been reported to have achieved more than 85% of its total size

at age five[30, 31]; therefore, the structures are not severely affected by growth and can be used as reference planes for adequate standardization and orientation.

Cevidanes at al.[26] have studied cranial base superimpositions using surface models of the cranial base. This allows obtaining separate displays of the cranial base, maxilla and mandible by establishing boundaries between anatomic structures. The way to assess registration is done differently for adults than for growing patients. In adults, the registration is done with the grey level CBCT data sets at the whole surface of cranial base. Since the sphenooccipital synchondrosis, the lateral wall of the skull and the frontal lobes and sinuses still have growth potential in growing patients there is a need for a different registration method.

First, the head is aligned by using the whole cranial base and then a finer registration at the stable structures on the anterior cranial base is used. The area selected is obviously smaller than in growing patients, but includes anatomical structures that have completed growth by age seven, such as: anterior wall of sella, anterior clinoid process, planum sphenoidale, lesser wings of the sphenoid, superior aspect of the ethmoid and

cribiform plates, cortical ridges on the medial and superior surfaces of the orbital roofs and inner cortical layer of the frontal bones.

The overlay of the 3-D model surfaces previously registered in the same coordinate system is then analyzed. Different degrees of transparencies to assess visually the boundries of the soft-tissue structures between superimposed models from two time points are then displayed with colored maps. The software (CMF software) calculates thousands of color coded distances in millimeters between before and after treatment 3-D models. Changes can be then visualized as displacements relative to the cranial base as seen on the color maps.

Image registration is not a simple task. Registration procedures are classified into rigid and nonrigid registrations. Rigid registrations include translation and rotation and they can be based on landmarks, semilandmarks, curves, planes, surfaces or voxels. This is a routine and acceptable way to evaluate longitudinal changes. Cevidanes used voxel-based registration on the cranial base on the before and after treatment images to evaluate these changes. On the other hand, non rigid registration includes translation,

rotation, scale and affine properties and can be based on more complex items such as elastic models, fluid models, splines, finite element models as well as landmarks[26].

Three-dimensional CBCT studies have investigated dental and skeletal outcomes of orthodontic treatment in different malocclusions. Sanders et al. (2010)[32] and Cachecho et al. (2012)[33] have used a three-dimensional identification of points in an x,y,z Cartesian coordinate system to assess differences in asymmetrical subjects. They also described a reliable method in longitudinal studies when comparing CBCT scans. This seems to be an optimal way of describing tooth movement in a maxillary superimposition after orthodontic therapy has been used. Two dimensional measurements are routinely affected by errors in landmark identification. So inevitably 3-D will have similar errors even though structures are identified in three planes using defined landmarks. Therefore there is a need to quantitate the accuracy and precision of 3-D landmarks measurements.

The purpose of the current study is to identify a reliable method for the superimposition of the nasomaxillary in a three-dimensional view using cone-beam computed tomography (CBCT). In order to do this, it is

necessary to establish stable landmarks in the nasomaxillary complex that do not change with growth, or that barely change with growth. The idea is to establish a constellation of landmarks within the nasomaxillary complex that 1) are reliable 2) are stable with growth and 3) that do not change in relationship with each other over time.

Superimposition of 3-D images might be an alternative method for analyzing and describing changes during and after treatment. With all the technology and imaging advances it remains challenging, as there is a difficulty of choosing and selecting landmarks, structures or areas as possible registration points that would not change during growth or orthodontic treatment.

With the advanced technology, the fact that 3-D imaging enables us to use voxel based registrations that may prove to be a superior method in the future. Our goal in this project is to identify possible landmarks so we could use the area within the desired landmark as a voxel size registration. The fact that more than one area in the maxilla remains unchanged with growth is the essence of superimposing by voxel registrations.

No literature has been published at this point about the application of applying the voxel-based registration in the maxilla or the mandible. It seems like a stable area where the voxel registration would be used, needs to be described and established first. One of the main goals in this study is to identify possible stable landmarks and assess the relationship within the landmarks themselves to see if they remain unchanged with time.

Literature Review Refererences:

1) Baumgaertel S. Reliability and accuracy of cone-beam computed tomography dental measurements. Am J Orthod Dentofacial Orthop 2009;136:19-2
2) Ricketts R. A Foundation for Cephalometric Communication. Am J Orthod 1960;46(5): 330-57
3) Hans, M. G. (2001). Three-Dimensional imaging: The Case Western Reserve University Method. Semin Orthod, 7:233-243.
4) Lagravère M.O., Low C, Flores-Mir C, Chung R, Carey J.P., Heo G., Major P.M. Intraexaminer and interexaminer reliabilities of landmark identification on digitized lateral cephalograms and formatted 3-dimensional cone-beam computerized tomography images. Am J Orthod Dentofacial Orthop 2010;137:598-604
5) Baumrind S, Frantz R. The reliability of head film measurements. 1. Landmark Identification. Am J Orthod 1971;60(2):111-127
6) Baumrind S, Frantz R. The reliability of head film measurements. 2. Conventional angular and linear measures. Am J Orthod 1971;60(5):505-517
7) Mu-Hsiung Chen, Jenny Zwei-Chieng Chang, Sang-Heng Kok, Yi-Jane Chen, Yao-Der Huang, Kai-Yuan Cheng, Chun-Pin Lin. Intraobserver reliability of landmark identification in cone-beam computed tomography-synthesized two-dimensional cephalograms versus conventional cephalometric radiographic: A

preliminary study. Journal Dental Sciences (2013), http://dx.doi.org/10.1016/j.jds.2013.02.012

8) De Oliveira AE, Cevidanes LH, Phillips C, Motta A, Burke B, Tyndall D. Observer reliability of three-dimensional cephalometric landmark identification on cone-beam computerized tomography. Oral Surg Oral Med Oral Pathol Oral Radiol Endod 2009;107:256-265

9) Papdopoulos M, Jannowitz C, Boettcher P, Henke J, Stolla R, Zeilhofer H, Kovacs L, Erhardt W, Biemer E, Papadopulos N. Three-dimensional fetal cephalometry: An evaluation of the reliability of cephalometric measurements based on three-dimensional recontructions and on dry skulls of sheep fetuses. J Cranio Maxill Surg 2005;33:229-237

10) Brown A, Scarfe W, Scheetz J, Silveira A, Farman A. Linear accuracy of cone beam CT derived 3D images. Angle Orthod 2009;79:150-157

11) Takeshi Sekiguchi, Bhim S. Savara. Variability of cephalometric landmarks used for growth studies. Am J orthod 1972;61(6):603-618

12) Ghafari, J. Cephalometric superimposition on the cranial base: a review and a comparison of four methods. Am J Orthod Dentofac Orthop 1987;91:403-13

13) Julius RB. A serial cephlometric study of the metallic implant technique and methods of maxillary and mandibular superimposition. [Thesis.] Seattle: University of Washington, 1971.

14) Bjork A. Facial growth in man studied with the aid of metallic implants. Acta Odontol Stand 1955;13:9-34.

15) Nielsen IL. Maxillary superimposition: a comparison of three methods for cephalometric evaluation of growth and treatment change, Am J Orthod Dentofac Orthop 1989;95(5):422-31.
16) Gu Yan, McNamara J. Cephalometric Superimpositions. Angle Orthodontist, Vol 78, No 6, 2008
17) Cook, A. et al. The variability and reliability of two maxillary and mandibular superimposition techniques. Part II. Am J Orthod 1994;106:463-71
18) Bjork A, Skieller V. Facial development and tooth eruption. Am J Orthod 1972;Vol 62(4):339-83
19) Bjork. Sutural growth of the upper face studied by the implant method. Acta Odontol Stand 1966;24:109-27
20) Baumrind, S. et al. Quantification of maxillary remodeling. 1. A description of osseous changes relative to superimposition on metallic implants. Am J Orthod Dentofacial Orthop 1987;91:29-41.
21) Baumrind, S. et al. Quantification of maxillary remodeling. 2. Masking of remodeling effects when an "anatomical" method os superimposition is used in the absence of metallic implants. Am J Orthod Dentofacial Orthop 1987;91:463-74
22) Lagravere M, Major P. Proposed reference point for 3-dimensional cephalometric analysis with cone-beam computerized tomography. Am J Orthod Dentofacial Orthop 2005;128:657-60

23) Doppel, D. et al. An investigation of the maxillary superimposition techniques using metallic implants. Am J Orthod Dentofac 1994;105:161-8
24) Houg A. A serial study of the constancy of relationship of maxillary cephalometric landmarks as viewed in the lateral headfilm. [Thesis.] Seattle: University of Washington, 1960.
25) Baumrind S, Miller D, Molthen R. The reliability of head film measurements. 3. Tracing superimposition. Am J Orthod 1976;70(6):617-644
26) Cevidanes L, Motta A, Proffit W, Ackerman J, Styner M. Cranial base superimposition for 3-dimensional evaluation of soft tissue changes. Am J Orthod dentofacial Orthop 2010;137:S120-9
27) Bjork A. Variations in the growth Pattern of the Human Mandible: Longitudinal Radiographic Study by the Implant Method. J dent Res 1963;42(Suppl 1):400-11
28) Lagravère M.O. Cranial base foramen location accuracy and reliability in cone-beam computerized tomography. Am J Orthod Dentofacial Orthop 2011;139:e203-e210.
29) Wu et al. "Establishing a superimposition method to compare results in pre- and post - treatment with CBCT: Part I: Stable cranial-base landmarks for three dimensional superimposition of CBCT" Master's Thesis 2011, Case Western Reserve University, Cleveland-OH
30) Lagravere M, Major P. Plane oritentation for standardization in 3-dimensional cephalometric

analysis with computerized tomography imaging. Am J Orthod Dentofacial Orthop 2006;129:601-4

31) Melsen B. The cranial base. Acta Odontol Scand 1974;32(Suppl 62)

32) Sanders D.A., Rigali P.H., Neace W.P., Uribe F., and Nanda R. Skeletal and dental asymmetries in Class II subdivision malocclusions using cone-beam computed tomography. Am J Orthod Dentofacial Orthop 2010;138:542.e1-542.e20

33) Cachecho et al. "A Three- Dimensional Evaluation of Class II Subdivision Malocclusion Correction" Master's Thesis 2011, Case Western Reserve University, Cleveland-OH

Statement of the thesis

The aim of this retrospective study is to describe the envelope of error, reliability and relative stability of landmarks in the nasomaxillary complex that may be used to isolate treatment effects in 3-D.

The aims of this project are to: 1) Identify reliable landmarks of the nasomaxillary complex using a cone-beam computed tomography (CBCT), 2) Describe their envelope of error 3) Identify stable landmarks of the nasomaxillary complex over time.

The hypotheses are:

1) The landmarks are not reliable in all three planes of space;

2) The landmarks are not relatively stable in time when evaluating all three planes of space;

3) The constellation of landmarks does not change in relationship to each other with time in all three planes of space.

The envelopes of error, reliability and stability of nasomaxillary landmarks to isolate treatment effects in 3-dimensions

Authors: Andrea Font Rytzner, D.D.S.[1]

Mark Hans, D.D.S., M.S.D.[2]

Juan Martin Palomo, D.D.S., M.S.D.[3]

Sena Narendran, B.D.S., D.D.P.H., M.Sc.[4]

Manish Valiathan, D.D.S., M.S.D.[5]

1. Resident, Department of Orthodontics at the School of Dental Medicine, Case Western Reserve University in Cleveland, OH
2. Professor and Chairman, Department of Orthodontics at the School of Dental Medicine, Case Western Reserve University in Cleveland, OH
3. Associate Professor and Program Director, Department of Orthodontics at the School of Dental Medicine, Case Western reserve University in Cleveland, OH
4. Associate Professor, Department of Community Dentistry at the School of Dental Medicine, Case Western reserve University in Cleveland, OH
5. Associate Professor and Program Director of the Craniofacial Fellowship program, Department of Orthodontics at the School of Dental Medicine, Case Western reserve University in Cleveland, OH

Corresponding Author:

Manish Valiathan, D.D.S., M.S.D.

Case Western Reserve University

School of Dental Medicine

Department of Orthodontics

10900 Euclid Ave.

Cleveland, OH 44106

mxv13@case.edu

The envelopes of error, reliability and stability of nasomaxillary landmarks to isolate treatment effects in 3-dimensions

OBJECTIVE: to describe the envelope of error, reliability and relative stability of landmarks in the nasomaxillary complex that may be used to isolate treatment effects in 3-D.

METHODS: Existing pre (T_1) and post (T_2) treatment CBCT volumes of 30 randomly selected adolescent patients' were oriented using cranial nerve canals to establish the 3 reference planes. Using a coordinate system, 10 landmarks were identified and the envelopes of error were plotted using scatter graphs. Reliability of all landmarks was assessed with ICC and scatter graphs. The IO, NPF, GPF landmarks were used to evaluate their relative stability and utility in isolating treatment effects.

RESULTS: The variation of the IO, LD and NPF were greater along the axial axis. The axial plane was the least reliable in all landmarks. There was no clear change of direction for most landmarks. The transverse dimension of the IO significantly increased with time. The vertical dimension increased the most variable from T_1 to T_2, especially for IO-GPF. The interdistances of IO, GPF and NPF for the most part was statistical significant.

CONCLUSION: Landmarks had characteristic envelopes of error in all three planes. Tested landmarks were reliable; the least reliable was the axial axis. GPF and NPF were relatively stable areas for future voxel-based superimpositions. Basion might not be a stable landmark over time.

Keywords: Envelope of error, Reliability, Coordinate, CBCT, Maxillary superimposition

Introduction

Cone beam computed tomography (CBCT) offers images of undistorted the dentition and other maxillofacial structures[1] used to visualize previously unseen information. Cephalometrics was used extensively in the previous century to understand facial growth and development. Ricketts[2] stated that one of the applications of cephalometrics is to record and to measure changes. Cephalometric superimpositions have been used to describe spatial changes of the craniofacial structures in 2-D[3-10]. Such superimpositions have been based in the implant studies that detected stable landmarks in 2-D[7-11].

The use of 3-D imaging promises to overcome some limitations of traditional 2-D cephalometrics, namely magnification and distortion errors. However, not all limitations could be overcome in 3-D. Baumrind and Frantz[12, 13] classified three major error groups: errors of projection, errors of identification and mechanical errors of measurements. The identification errors and mechanical errors in measurement remain a challenge to be overcome in 3-D. Baumrind and Frantz quantified the precision of different landmarks used in 2-D cephalometrics with scatter grams to assess landmark identification errors. They concluded that the errors were too great to be ignored with the magnitude of error varying depending on the landmark and the distributions of errors were not random, but rather systematic. Every landmark has a characteristic and usually noncircular envelope of error.

Intraexaminer and interexainer reliability between CBCT synthesized 2-D cephalograms versus conventional cephalometric radiography have been compared[13,

[14]. Some landmarks were found to have lower identification reliability in 2-D cephalograms synthesized from CBCT. Several methods of maxillary superimposition have been described in the literature[3, 7, 15-17]. Depending on the registration points used, potentially erroneous information concerning patterns of growth and dental movements may result[15, 16, 18].

Orientation of 3-D volumes, the first step prior to landmark identification, has been previously described by Lagravère et al.[19, 20] who tested the accuracy and reliability of cranial base foramen locations in CBCT scans. Foramina spinosum, ovale, rotundum and the hypoglossal canal were reported as acceptable landmarks to use in establishing reference coordinate systems for 3-D superimposition. Wu et. al[21] developed an optimal and reliable way of orienting the head based on cranial nerves.

A most recent method of superimposing to assess treatment changes based on voxel-based registration has been described by Cevidanes et. al [22]. They used surface models of the cranial base obtaining separate displays of the cranial base, maxilla and mandible by establishing boundaries between anatomic structures.

Three-dimensional CBCT studies have investigated dental and skeletal outcomes of orthodontic treatment in different malocclusions using identification of points in an X, Y, Z Cartesian coordinate system [23, 24]. The coordinate system proved to be reliable for the longitudinal study of Class II subdivision malocclusion treatment changes as well as the evaluation of skeletal and dental asymmetries[25]. There is a need to quantitate the accuracy and precision of 3-D landmark measurements. The purpose of the current study is to attempt to describe the envelope of error, reliability

and relative stability of landmarks in the NM complex that may be used to isolate treatments effects in 3-D.

Materials and Methods:

Initial and final records were identified from a pre-existing data base of patients treated in the graduate orthodontic department at the clinic institution. Existing patient records included T_1 and T_2 treatment intraoral/extraoral photographs, study models and Cone Beam Computed Tomography scans (CB MercuRay, Hitachi Medical Systems America Co. – Twinsburg, OH) using the 2mA setting and the largest field of view (0.38mm Voxel size). Sample size calculations were based on two tailed alpha, α=0.05 and β=0.2. The Expected Effect Size (E) was set at 0.5mm and the standard deviation (SD) of 0.64 was based on the study by Wu et. al[21]. Based on the sample size calculation (E/S=0.78), a minimum of 25 subjects were required. Institutional Review Board approval was obtained, and informed consent forms were signed by all subjects.

The inclusion criteria were: 1) patients between 11-16 years old at the time of initial orthodontic records that started the treatment after 2009; 2) availability of CBCT scans at the time of records, dental and medical histories and complete treatment notes; 3) basion within the field of view of CBCT taken at T_1 and T_2; 4) patients with bilateral Angle class I molar relationships. The exclusion criteria were patients who: 1) had previous orthodontic treatment; 2) craniofacial anomalies or syndromes; 3) noted rapid palatal expander (RPE) or archwire expansion; 4) extraction of permanent teeth; 5) patients treated with a headgear device; 6) treated with maxillary protraction, molar distalization appliances or temporary anchorage devices (TAD's).

A total of 66 charts out of a pool of 177 patients that matched the inclusion criteria were reviewed. The first 30 randomly selected patients that met the inclusion criteria formed the sample and 36 were excluded for failing to meet the inclusion criteria prior to establishing the sample.

Ten landmarks were used and evaluations of their envelopes of errors were constructed. Reliability and relative stability to each other with the intent to isolate changes in the nasomaxillary complex were evaluated. Eight landmarks were bilateral and two midline landmarks were assessed. The bilateral landmarks and methods of measuring them are:

- **Infraorbitale Foramen (IO)**: the most superior part of the foramen identified first in the sagittal slice. The most distal edge of the foramen in the axial view was located and the landmark was placed to coincide in the sagittal and axial view. In the coronal slice, the landmark will always be in the distal view of the foramen (Figure 1).
- **Lacrimal Duct (LD)**: the location of the lacrimal right and left radiolucency (RL) in the coronal slice by tilting the head such that the axial reference line passed through the center of both RL was first identified (Figure 2). Visualization of the right RL in the sagittal slice and placement of the landmark in the highest point of the RL was achieved. Volume was set at the current slices and with the symmetry caliper set in the horizontal plane of the 3-D volume view, the landmark is moved until the first contact with the frontal process of the maxilla. This allowed coordinates on bone, as the lacrimal duct is RL, the measurements that would be retrieved would not be

consistent. To achieve the location of the left side, using the symmetry caliper upon the right landmark previously plotted, we selected the intersection with the caliper and the most lateral point of the frontal process of the left maxilla.

- **Nasopalatine Foramen (NPF)**: the most posterior part of the foramen as seen in the sagittal view was located first and the axial reference line was placed on that mark. Then in the axial slice, the sagittal and coronal reference lines were located in the center of the foramen allowing a clear view of the canal on the coronal slice. Both landmarks were placed on the axial reference line when in contact to the inner cortical surface of the canal on the coronal slice.
- **Greater Palatine Foramen (GPF)**: location of the GPF was first identified in the coronal slice. The coronal plane was scrolled from inferior to superior until a clear outline of both foramina was seen in the axial plane (Figure 6). Then the head was rotated to align the center of both foramina. The tilt of the head was modified so that the floor of the nose in the coronal slice was parallel to the axial line. The landmark was then placed across the axial reference line when in contact with the most medial point of the canal (Figure 7).

The midline landmarks are:

- **Anterior Nasal Spine (ANS)**: the most anterior part where the right and left maxilla meet.
- **Posterior Nasal Spine (PNS)**: the most posterior part where the right and left palatal bones meet.

The 3-D image orientation method described by Wu et al.[13] was used to orient T_1 and T_2 CBCT images. In the coronal view (Figure 8), the axial plane was aligned with the center of the left and right optical foramina by tilting the head. In the axial view the coronal plane was aligned with the center of the left and right foramina ovale by rotating the head (Figure 9) and then the axial plane was scrolled to the level of foramen cecum (Figure 10). The sagittal plane was positioned to pass through foramen cecum. Finally, in the sagittal view, the pitch of the head was adjusted so that the axial plane overlapped McRae's line (Basion to Opisthion) as seen in Figure 11. This process allows the image to be fixed in the three planes of space and without rotating the image in any direction; the axial plane overlapping McRae's line and the sagittal plane overlapping foramen cecum, the coronal plane was set at Basion. The Origin, or (0,0,0) coordinate, was estimated at Basion where all 3 planes intersect. This orientation and coordinate system was saved as default orientation, allowing the operator to reset it between every landmark registration.

All skeletal landmarks were placed on T_1 and T_2 treatment CBCT's and registered digitally using the program Dolphin 3-D (version 11.0 premium software) by one operator on the volume slices on the CBCT image that were oriented using Wu's method[21]. The 3-D virtual rendering was mainly used as a general overview of the registration, not for landmark placement, with the exception of the lacrimal duct to avoid placement in air.

Each landmark, once identified, was represented by values in an X,Y,Z Cartesian coordinate system. The three values for each landmark were exported into Microsoft Excel (Microsoft, 2010) where X, Y, Z coordinates were registered and

measurements in mm were calculated. Landmarks from all 60 volumes (T_1 and T_2) were used to create scatter graphs and describe the envelopes of error for each landmark. To test reliability, a third of the sample (20 volumes) was randomly selected and landmarks were re-plotted a total of three times with an interval of minimum two weeks between landmark placements. All volumes were reoriented from the raw dicom file prior to new landmark placement. Landmarks were placed without visualizing previous measurements. Reliability was tested using these data and by creating scatter graphs as well as using the interclass correlation coefficient (ICC). The X, Y, Z values of the reliability subjects were averaged for a best estimate for each landmark, and that was considered the "true landmark value" for this study.

The scatter plots were analyzed in all three planes of space, and the three most reliable landmarks were chosen for further analysis of inter-distance measurements and relative stability. The right and left infraorbital foramina (IO), greater palatine foramina (GPF) and nasopalatine foramen landmarks (NPF) were chosen (six landmarks in total, all being bilateral). Distances in relationship to each other (IO-GPF, GPF-NPF, and NPF-IO) were measured for each side and compared using t-test between T_1 and T_2. Distances between the right and left side were also measured for each landmark to assess transverse change.

All descriptive statistics were calculated using Statistical Package for Social Sciences (SPSS 20.0, Inc.-Chicago, IL). Distances between landmarks were measured in mm, as well as means, absolute values and standard deviations (SD). The landmarks were defined as perpendicular measurements from each 3-D landmark to each of the 3-D coordinate system as described in Sanders at al. in 2010[23]. Distances

between the landmarks at T_1 were compared to distances between the same landmarks at T_2 to assess any changes in relation to each other.

Results

The study sample consisted of thirty treated Class I malocclusion subjects. Of the thirty subjects, there were 16 females and 14 males ranging in age from 11 years and 4 months to 17 years and 7 months (Table 1). The mean age at T_1 was 13.56 $\pm$1.18 and 15.61$\pm$1.06 at T_2. The average treatment time was 2.05$\pm$0.43 years.

All spatial changes are represented in the following manner: changes in the X plane (sagittal plane) reflect transverse changes; the Y plane (axial plane) reflects vertical changes and the Z plane (coronal plane) reflect the anterior-posterior changes. Histograms representing normal distributions were made for all variables in all three planes of space. All followed a bell shaped curve indicating normal distribution, with the exception of outliers in the sagittal plane for the IOL, NPFR, PNS, in the axial plane for the IOR and the coronal plane for NPFR and NPFL. All coordinate data were evaluated considering Basion as the coordinate of origin. The assumption that Basion is stable in the age group of this study was made, therefore all data is expressed relative to Basion.

Scattergrams show the distribution of estimated errors in three planes of space resulting in 3 graphs representing each landmark (Figures 12-16). Data from T_1 and T_2 of all subjects were used to construct these scattergrams, therefore a total of 60 plots are represented in each graph. The variation of the IO, LD and NPF are greater along the axial axis than the coronal and sagittal axis. The distribution of estimated errors follows the same distribution of error for ANS and PNS. The dispersion in the coronal axis for the GPF is greater than in the axial and sagittal axis, but the envelope

of error follows a circular pattern. All bilateral landmarks followed the same envelope of error for the right and left side.

Intraclass correlation coefficient (ICC) was measured on a third of the sample a total of 3 times (Table 2). All landmarks were highly reliable in all planes. The least reliable was the X axis in PNS. The same reliability data was also represented by scatter graphs. First, they were visually compared to the scatter grams of the entire sample and similar patterns of distribution of error were appreciated in all planes of space. Second, they represent reliability within the same landmark. The closer the plots are, the more reliable they were (Figures 17-21). The greatest variation in reliability on both the right and left IO foramen is the axial plane (Figure 17). The axial plane is also the least reliable in the NPF and GPF, while in the coronal plane, there is an increase in range of scatter plots, but seems to follow a particular circular pattern (Figures 19, 21). In regard to ANS and PNS, there was a similarity in the pattern of reliability in all three planes of space (Figure 20).

Means and SD were calculated using the "true landmark value" for each landmark as well as the estimated error (Table X). The distribution according to the direction of change for all landmarks is presented in Table 3. There was no clear cut change of direction for most landmarks. However, both IO landmarks in the sagittal axis had a general tendency to move away from the midline. For the GFP, the sagittal axis also had a tendency to move away from the midline (4 out of 30 subjects had no change). In the coronal axis, all landmarks tended to move in a forward direction, except for PNS which tended to move in a backward direction. To a lesser extent, the

GPF also tended to move in a backward direction. The general tendency in the axial plane was to move downwards.

The amount of change between T_1 and T_2 can be seen on Table 4 (means and SD). This is based on absolute values, so the direction of change would not influence the true mean. It can be appreciated that the axial plane of all landmarks has the higher mean, suggesting that the axial axis was the most variable from T_1 to T_2. Outliers above two standard deviations were removed as reported on previous findings[8, 11, 12]. Even though the sagittal axis of the IO tended to move away from the midline, the absolute mean of the difference between T_1 and T_2 was the lowest of all landmarks 0.6 $\pm$ 0.49mm (with the exception of LD). Among the IO and NPF landmarks, the variability was high in the axial plane.

The IOF, NPF and GPF landmarks were used as a constellation of landmarks to assess differences between each other. Average distances from T_1 to T_2 between IO-NPF, NPF-GPF and IO-GPF in all three planes of space for the right and left side are presented in Table 5. All mean differences were 1mm or less, except for the IO-GPF in the axial plane (1.08 $\pm$ 0.89 and 1.30 $\pm$ 1.11mm for the right and left side respectively). Paired t-tests were used to compare these distances between themselves for all three dimensions. Distance changes from T_1 to T_2 comparing IO-NPF, NPF-GPF and IO-GPF for the right and left side are shown in Table 6. Most of the distances between these landmarks showed a statistical significant change, except for the Y axis between GPF and NPF bilaterally.

Comparison of both sides was used to assess transverse changes. Paired t-tests were used to compare the differences in distance between landmarks at T_1 and T_2 between the right and the left sides were used as a constellation (Table 7): IOF, NPF and GPF. Only the distance between the right and left IOF showed a significant change in the axial plane ($p<0.05$).

Discussion

Scatter-plots were used to demonstrate the distribution pattern of landmark identification errors[11, 12, 14]. Our scatter grams agree with Baumrind's[11] findings that there are large differences in reliability of estimation of landmarks in particular planes (see Figures 12-16). Baumrind et al.[11] stated that errors in landmark identification are too great to be ignored and that the magnitude of error varies greatly form landmark to landmark representing distribution of errors that seems systematic, depending on each landmark. Our findings are not exempt from the same errors found in 2-D.

The distribution of errors of the IO, LD, NPF and GPF has not been described in the literature. The estimates of IO, LD and NPF are distributed primarily along the axial plane suggesting the difficulty of identifying landmarks in this dimension. Head orientation in CBCT imaging is critical. The fact that opisthion has a variability of the axial position influences McRae's line, which is used as a standard measurement in the orientation method[21, 24]. Thus, for every patient, the result of the "pitch" of the head would differ. More studies perhaps clarifying the orientation method for the axial axis should be further investigated. This difference in every patient could explain the large variability seen along the axial plane in the scatter graphs. Basion was considered a stable landmark over time; the results in this study suggest that this assumption is incorrect and should be kept in mind in future studies.

If the estimation of the landmark represented a gradual curve and not a sharp edge, the errors tend to be larger and distributed along the edge itself [11]. These

findings agree with our scatter plots in the manner of those that are most dispersed seemed to be the landmarks located on undefined surfaces when landmark identification was taken place. Locating 3-D landmarks on complex anatomical structures is prone to more identification error than those registered in a 2-D fashion[22].

Sekoguchi[26] discussed variations in landmark location and how to minimize variability for these structures. Orbitale has been described to be more variable in the horizontal plane than the vertical plane in 2-D cephalometrics[26]. The IO landmark used in this study (below orbitale), suggest that the axial axis was the most variable. Perhaps Sekoguchi's findings are consistent with the fact that orbitale is found on a surface distributed along the horizontal axis on 2-D cephalograms. For the IO foramen landmark however, the axial variation could possibly be explained by the variation of the pitch of the head during orientation. It could also be explained by the anatomically variability between subjects as to where the IO foramen lies. In the sagittal plane, there is a correlation with age to the distance of the infraorbital foramen from the midline[27]. It has also been reported that the range from the infraorbital rim to the infraorbital foramen can be as large as 3mm-15mm[28], so the anatomical variation can affect the variability in the axial plane.

Other authors have described[29, 30] the necessity to be more precise when identifying landmarks in 3-D. Ideal locations for landmarks in CBCT such as edges, foramina and apices have been described previously[13]. Though foramina are used as landmarks, they are still subject to landmark identification error primarily due to the

fact that it needs to be located in all three planes of space, and not all axes have a clear view or description of the particular landmark.

Landmarks used in the current study are a representation of the nasomaxillary complex and not just the maxilla. Bjork[10] described the stability of the mandibular nerve canal during growth and the assumption that most nerve canals do not change in time was made for landmark selection. A similar assumption was made in the current study.

ANS and PNS were not used in the constellation of landmarks. Superimposition on the palatal plane has been previously based on ANS and PNS. Steiner[17] pointed out the underestimation of the eruption of the dentition by 30%-50% as well as the masking of the downward remodeling of the maxilla and palate when superimposing on ANS or PNS. He defined PNS as an unstable area, as it alters during growth. Lagravere[13] and Papadopoulos[30] suggested that areas with low density make it harder to identify such landmarks, like ANS or PNS. Several methods of maxillary superimposition have been described in the literature[15, 16]. Depending on the registrations used, erroneous information concerning patterns of bone growth and remodeling can be obtained, as well as distortion of tooth movements[7, 15, 16, 18]. Our results agree with Baumrind in the manner of the direction of change in the lateral and axial direction of ANS[8]. The tendency of PNS to move backwards, and ANS to move forward, is consistent with other studies in the matter of the anteroposterior direction of growth[6, 8, 31].

The LD was excluded for the following reasons: first, the envelope of error in the axial axis was too great to consider the landmark as a potential area for superimposition. Second, the fact that so many outliers were present in the axial axis, made the absolute value of the difference between T_1 and T_2 suggest that the area is not stable in time. This might be explained by its proximity to the frontal suture, where nasomaxillary changes occur. Changes from T_1 to T_2 in the sagittal and axial axis of the IO-NPF distances and the IO-GPF distances for both the right and left may be a limitation to the current study. The axial changes may be related to the orientation method used in this study, or to the anatomical variation in the location of IO foramen.

Natural craniofacial growth might suggest an alternative explanation. The development in height takes place by sutural growth and appositional growth of the alveolar process in combination with a resorptive lowering of the nasal floor[4, 8]. Baumrind et al.[8] assessed cumulative changes on the magnitude and pattern of remodeling of the superior and anterior surfaces of the maxilla viewed on a 2-D lateral cephalogram. The superior surface of the maxilla was found to remodel downward with a tendency towards a forward rotation of the maxilla[8, 17]. Our findings suggest that the IO-NPF distances are not relatively stable in the axial plane, suggesting that as the lowering of the nasal floor and the deposition of the hard palate occurs, it seems consistent that the NPF will follow a downward direction in time, and perhaps remodels at a different rate in time than the IO.

Bjork[9] and Melson[31] reported the increase in transverse dimension in the maxilla. It is no surprise then that the transverse dimensional changes reported in this study at the IO increased with time are consistent with normal facial growth. Using metallic implants and maxillary superimpositions, Julius[17] noted parallelism and the approximate location of the posterior and key ridge surfaces of the maxillary zygomatic process; an anterior and vertical location on the infraorbital foramen and a clockwise rotation and remodeled lowering of the palatal plane. In the present study, the general tendency of the IO was to remodel posteriorly and upwards.

Doppel[7] found that the internal structure of the palate could be a promising area of stability. Limitations were perceived due to the difficulty in registering structures within the internal maxilla. We may have contributed to the methodology by testing reliability of NPF, as this landmark is in the anterior internal maxillary area. The zygomatic process of the maxilla was found to be the most stable anatomic landmarks when tracing lateral cephalograms of maxillary superimpositions based on metallic implant registrations[7]. However, the zygomatic process is a complex structure that has no reported landmark associated for analyses in 3-D. Perhaps landmarks need to be identified and defined in this area. The infraorbital foramen, pterygomaxillary fissure (PTM), ANS, PNS, A point and the superior and inferior borders of the palate were found unreliable for maxillary superimpositions[7]. Doppel had similar findings to ours when comparing orbitale and IO. The floor of the orbit arises more than the palatal plane lowers in a ratio of 1.5 to 1mm. This agrees with

our findings in relationship to the infraorbital foramen, where the general tendency was for the IOF to remodel upwards.

The fact that most distances between IOF, GPF and NPF from T_1 to T_2 are statistical significant might suggest that these areas might remodel at a different rates from each other. The average difference from the distance IO-GPF for the right and the left sides may not be clinically significant[13, 14] given the landmark error, identification and/or orientation errors. Consistent and reproducible data can be obtained with operator training and calibration. Experience must be taken into account on behalf of the operator, since 3-D reconstruction and image reading is not the same as 2-D and therefore caution should be taken into account when selecting planes to locate different landmarks.

The limitation of using landmark based cephalometrics when using 3-D imaging is that even with angular and linear measurements involved, there is a clear inability of assessing how surfaces change rather than how specific points change in time. Cevidanes et al.[22] used entire anatomical surfaces for voxel-size superimpositions. Our objective with this study was to assess possible local areas in the NM complex for future superimposition studies using voxel-based models. Further studies need to be made applying these structures as local areas of superimposition using voxel-based superimposition.

Conclusions

During growth, landmarks are expected to change when using a coordinate system. More precise definition should be taken into account when describing 3-D landmarks in all three planes of space to further increase reliability. It appears that there is no area in the NMC that is completely stable.

1. All landmarks had a characteristic envelope of error in all three planes of space.
2. All landmarks were reliable in all three planes of space.
3. IO, NPF, GPF were relatively stable in time. Only sagittal in IO significantly increased with time. Variability of IO and NPF was highest in the axial axis.
4. Distances between: IO-GPF, IO-NPF and GPF-NPF were statistically significant in time, suggesting different remodeling rates.
5. GPF and NPF seem to suggest relatively stable areas for future voxel-based superimpositions. The variability of IO suggests that future studies may considerate alternate areas to IO.
6. The LD was reliable, but not stable in time.
7. The results in this study may suggest that Basion is not stable in time.

Further studies with using these landmarks to assess maxillary superimposition must be undertaken. Studies based on a limited area for voxel size registration need to be evaluated using these landmarks. Additional landmarks may need to be investigated prior to isolating treatment effects in 3-D.

Manuscript References

1) Baumgaertel S. Reliability and accuracy of cone-beam computed tomography dental measurements. Am J Orthod Dentofacial Orthop 2009;136:19-2
2) Ricketts R. A Foundation for Cephalometric Communication. Am J Orthod 1960;46(5): 330-57
3) Bjork A. Facial growth in man studied with the aid of metallic implants. Acta Odontol Stand 1955;13:9-34.
4) Bjork A, Skieller V. Facial development and tooth eruption. Am J Orthod 1972;Vol 62(4):339-83
5) Bjork. Sutural growth of the upper face studied by the implant method. Acta Odontol Stand 1966;24:109-27
6) Baumrind, S. et al. Quantification of maxillary remodeling. 2. Masking of remodeling effects when an "anatomical" method os superimposition is used in the absence of metallic implants. Am J Orthod Dentofacial Orthop 1987;91:463-74
7) Doppel, D. et al. An investigation of the maxillary superimposition techniques using metallic implants. Am J Orthod Dentofac 1994;105:161-8
8) Baumrind, S. et al. Quantification of maxillary remodeling. 1. A description of osseous changes relative to superimposition on metallic implants. Am J Orthod Dentofacial Orthop 1987;91:29-41.

9) Bjork A, Skieller V. Growth of the Maxilla in Three Dimensions as Revealed Radiographically by the Implant method. Brit J Orthod. YEAR Vol 4(2); 53-64

10) Bjork A. Variations in the growth Pattern of the Human Mandible: Longitudinal Radiographic Study by the Implant Method. J dent Res 1963;42(Suppl 1):400-11

11) Baumrind S, Frantz R. The reliability of head film measurements. 1. Landmark Identification. Am J Orthod 1971;60(2):111-127

12) Baumrind S, Frantz R. The reliability of head film measurements. 2. Conventional angular and linear measures. Am J Orthod 1971;60(5):505-517

13) Lagravère M.O., Low C, Flores-Mir C, Chung R, Carey J.P., Heo G., Major P.M. Intraexaminer and interexaminer reliabilities of landmark identification on digitized lateral cephalograms and formatted 3-dimensional cone-beam computerized tomography images. Am J Orthod Dentofacial Orthop 2010;137:598-604

14) Mu-Hsiung Chen, Jenny Zwei-Chieng Chang, Sang-Heng Kok, Yi-Jane Chen, Yao-Der Huang, Kai-Yuan Cheng, Chun-Pin Lin. Intraobserver reliability of landmark identification in cone-beam computed tomography-synthesized two-dimensional cephalograms versus conventional cephalometric radiographic: A preliminary study. Journal Dental Sciences (2013), http://dx.doi.org/10.1016/j.jds.2013.02.012

15) Nielsen IL. Maxillary superimposition: a comparison of three methods for cephalometric evaluation of growth and treatment change, Am J Orthod Dentofac Orthop 1989;95(5):422-31.

16) Gu Yan, McNamara J. Cephalometric Superimpositions. Angle Orthodontist, Vol 78, No 6, 2008

17) Julius RB. A serial cephlometric study of the metallic implant technique and methods of maxillary and mandibular superimposition. [Thesis.] Seattle: University of Washington, 1971.

18) Cook, A. et al. The variability and reliability of two maxillary and mandibular superimposition techniques. Part II. Am J Orthod 1994;106:463-71

19) Manuel O. Lagravère. Cranial base foramen location accuracy and reliability in cone-beam computerized tomography. Am J Orthod Dentofacial Orthop 2011;139:e203-e210.

20) Lagravere M, Major P. Plane oritentation for standardization in 3-dimensional cephalometric analysis with computerized tomography imaging. Am J Orthod Dentofacial Orthop 2006;129:601-4

21) Wu et al. "Establishing a superimposition method to compare results in pre- and post -treatment with CBCT: Part I: Stable cranial-base landmarks for three dimensional superimposition of CBCT" Master's Thesis 2011, Case Western Reserve University, Cleveland-OH

22) Cevidanes L, Motta A, Proffit W, Ackerman J, Styner M. Cranial base superimposition for 3-dimensional evaluation of soft tissue changes. Am J Orthod dentofacial Orthop 2010;137:S120-9

23) Derek A. Sanders, Paul H. Rigali, William P. Neace, Flavio Uribe, and Ravindra Nanda. Skeletal and dental asymmetries in Class II subdivision malocclusions using cone-beam computed tomography. Am J Orthod Dentofacial Orthop 2010;138:542.e1-542.e20

24) Cachecho et al. "A Three- Dimensional Evaluation of Class II Subdivision Malocclusion Correction" Master's Thesis 2011, Case Western Reserve University, Cleveland-OH

25) Minich C, Araujo E, Behrents R, Buschang P, Tanaka O, Kim K. Evaluation of skeletal and dental asymmetries in Angle Class II subdivision malocclusions qith cone-beam computed tomography. Am J Orthod Dentofacial Orthop 2013;144:57-66

26) Takeshi Sekiguchi, Bhim S. Savara. Variability of cephalometric landmarks used for growth studies. Am J orthod 1972;61(6):603-618

27) Suresh A, Voronov P, Curran J. Infraorbital nerve Block in Children: A Computerized Tomography Measurement of the Location of the Infraorbital Foramen. Reg Anesth Pain Med 2006;31:211-14

28) Aziz S, Marchena J, Puran A. Anatomical Characteristics of Infraorbital Foramen: A Cadaver Study. J Oral Maxillofac Surg 2000,58:992-996

29) De Oliveira AE, Cevidanes LH, Phillips C, Motta A, Burke B, Tyndall D. Observer reliability of three-dimensional cephalometric landmark identification on cone-beam computerized tomography. Oral Surg Oral Med Oral Pathol Oral Radiol Endod 2009;107:256-265

30) Papdopoulos M, Jannowitz C, Boettcher P, Henke J, Stolla R, Zeilhofer H, Kovacs L, Erhardt W, Biemer E, Papadopulos N. Three-dimensional fetal cephalometry: An evaluation of the reliability of cephalometric measurements based on three-dimensional recontructions and on dry skulls of sheep fetuses. J Cranio Maxill Surg 2005;33:229-237

31) Melsen B. The cranial base. Acta Odontol Scand 1974;32 (Suppl 62)

APPENDICES

A. IRB approval from CWRU

CASE WESTERN RESERVE UNIVERSITY EST. 1826

NOTICE OF APPROVAL

CWRU IRB Protocol Number:	**IRB-2012-355**
Protocol Title:	***A determination of reliable and stable landmarks that may be used to detect treatment effects in three dimensions in the maxilla using cone-beam computed tomography (CBCT).***
Responsible Investigator (RI):	**Manish Valiathan**
Co-Investigator (CI):	**Andrea Font**
RI Department:	**Orthodontics**
Type of Review:	**Expedited**
Risk Level:	**Minimal**
Vulnerable Population(s):	**Children**
Approval Date:	**03/15/2013**
CONTINUING REVIEW DEADLINE:	**02/28/2014**
EXPIRATION DATE:	**03/14/2014**

The CWRU Institutional Review Board (IRB) has approved the above new protocol through the **EXPEDITED** review process.

When conducting Human Subjects' Research, your responsibilities include the following:

1. Report all adverse events and unanticipated problems involving human subjects to the IRB Office, located in the Office of Research Administration (ORA), within three (3) business days of your knowledge of the occurrence.
2. Provide the IRB with a complete Continuing Review form (available in our electronic application system at http://sberirb-app.case.edu, or from the ORA) by the continuing review deadline noted above, and when the study is to be terminated.
3. Submit all proposed changes to the protocol to the IRB and wait for IRB approval before implementing any protocol change or modification.
4. Keep all research data and original consent documents in your possession for at least three (3) years after the study is terminated.
5. Note that completely de-identified data can be kept and used for research indefinitely. The IRB is primarily concerned about identifiers/identifiable data. If you want to terminate your study, identifiers/identifiable data must be destroyed. This includes paper or electronic master lists, contact lists, codes/codebooks, transcripts containing identifiers and video and audio recordings.
6. If applicable, please use the most current IRB-approved consent forms. Feel free to use copies of these forms as long as they are identical to what was originally IRB approved. If you wish to change the forms or any other part of the study, you must submit an addendum request/protocol modification with revised copy(ies) of the relevant document(s) and wait for IRB approval before a modification can be implemented.
7. ***Discontinue all work pertaining to this protocol if a continuing review approval is NOT finalized by the expiration date noted above.*** No further work on this protocol is allowable until the proper continuing review materials or required revisions are approved by the IRB.

    a. Please note that, if the continuing review materials or required revisions are not received by the expiration date, the RI and this study would be automatically placed on Administrative Hold for 30 days. This means that the RI loses their IRB privileges and research from this study must cease.
    b. If after 30 days, the Case IRB still does not have the protocol for processing, this protocol will be administratively terminated and your IRB privileges will be revoked for all your protocols.

Thank you for your attention to this matter. Please contact the IRB office at 216-368-6993 if we can be of further assistance.

American Association of Orthodontists, patient Informed Consent p.1

INFORMED CONSENT

for the Orthodontic Patient

Risks and Limitations of Orthodontic Treatment

Successful orthodontic treatment is a partnership between the orthodontist and the patient. The doctor and staff are dedicated to achieving the best possible result for each patient. As a general rule, informed and cooperative patients can achieve positive orthodontic results. While recognizing the benefits of a beautiful healthy smile, you should also be aware that, as with all healing arts, orthodontic treatment has limitations and potential risks. These are seldom serious enough to indicate that you should not have treatment; however, all patients should seriously consider the option of no orthodontic treatment at all by accepting their present oral condition. Alternatives to orthodontic treatment vary with the individual's specific problem, and prosthetic solutions or limited orthodontic treatment may be considerations. You are encouraged to discuss alternatives with the doctor prior to beginning treatment.

Orthodontics and Dentofacial Orthopedics is the dental specialty that includes the diagnosis, prevention, interception and correction of malocclusion, as well as neuromuscular and skeletal abnormalities of the developing or mature orofacial structures.

An orthodontist is a dental specialist who has completed at least two additional years of graduate training in orthodontics at an accredited program after graduation from dental school.

American Association of **Orthodontists**

American Association of Orthodontists, patient Informed Consent p.3,

Consent to Use of Records

Patient _____ Date _____

Allergies
Occasionally, patients can be allergic to some of the component materials of their orthodontic appliances. This may require a change in treatment plan or discontinuance of treatment prior to completion. Although very uncommon, medical management of dental material allergies may be necessary.

General Health Problems
General health problems such as bone, blood or endocrine disorders, and many prescription and non-prescription drugs (including bisphosphonates) can affect your orthodontic treatment. It is imperative that you inform your orthodontist of any changes in your general health status.

Use of Tobacco Products
Smoking or chewing tobacco has been shown to increase the risk of gum disease and interferes with healing after oral surgery. Tobacco users are also more prone to oral cancer, gum recession, and delayed tooth movement during orthodontic treatment. If you use tobacco, you must carefully consider the possibility of a compromised orthodontic result.

Temporary Anchorage Devices
Your treatment may include the use of a temporary anchorage device(s) (i.e. metal screw or plate attached to the bone.) There are specific risks associated with them.

It is possible that the screw(s) could become loose which would require its/their removal and possibly relocation or replacement with a larger screw. The screw and related material may be accidentally swallowed. If the device cannot be stabilized for an adequate length of time, an alternate treatment plan may be necessary.

It is possible that the tissue around the device could become inflamed or infected, or the soft tissue could grow over the device, which could also require its removal, surgical excision of the tissue and/or the use of antibiotics or antimicrobial rinses.

It is possible that the screws could break (i.e. upon insertion or removal.) If this occurs, the broken piece may be left in your mouth or may be surgically removed. This may require referral to another dental specialist.

When inserting the device(s), it is possible to damage the root of a tooth, a nerve, or to perforate the maxillary sinus. Usually these problems are not significant; however, additional dental or medical treatment may be necessary.

Local anesthetic may be used when these devices are inserted or removed, which also has risks. Please advise the doctor placing the device if you have had any difficulties with dental anesthetics in the past.

If any of the complications mentioned above do occur, a referral may be necessary to your family dentist or another dental or medical specialist for further treatment. Fees for these services are not included in the cost for orthodontic treatment.

Patient or Parent/Guardian Initials _____

ACKNOWLEDGEMENT

I hereby acknowledge that I have read and fully understand the treatment considerations and risks presented in this form. I also understand that there may be other problems that occur less frequently than those presented, and that actual results may differ from the anticipated results. I also acknowledge that I have discussed this form with the undersigned orthodontist(s) and have been given the opportunity to ask any questions. I have been asked to make a choice about my treatment. I hereby consent to the treatment proposed and authorize the orthodontist(s) indicated below to provide the treatment. I also authorize the orthodontist(s) to provide my health care information to my other health care providers. I understand that my treatment fee covers only treatment provided by the orthodontist(s), and that treatment provided by other dental or medical professionals is not included in the fee for my orthodontic treatment.

Signature of Patient/Parent/Guardian Date

Signature of Orthodontist/Group Name Date

Witness Date

CONSENT TO UNDERGO ORTHODONTIC TREATMENT

I hereby consent to the making of diagnostic records, including x-rays, before, during and following orthodontic treatment, and to the above doctor(s) and, where appropriate, staff providing orthodontic treatment prescribed by the above doctor(s) for the above individual. I fully understand all of the risks associated with the treatment.

AUTHORIZATION FOR RELEASE OF PATIENT INFORMATION

I hereby authorize the above doctor(s) to provide other health care providers with information regarding the above individual's orthodontic care as deemed appropriate. I understand that once released, the above doctor(s) and staff has(have) no responsibility for any further release by the individual receiving this information.

CONSENT TO USE OF RECORDS

I hereby give my permission for the use of orthodontic records, including photographs, made in the process of examinations, treatment, and retention for purposes of professional consultations, research, education, or publication in professional journals.

Signature Date

Witness Date

I have the legal authority to sign this on behalf of

Name of Patient

Relationship to Patient

Notes

B. List of Tables

Table 1: Descriptive statistics

Table 2: Interclass correlation coefficient (ICC) for all landmarks

Table 3: Subject distribution according to the direction of change for all landmarks

Table 4: Descriptive statistics of the absolute value of the difference between T_1 and T_2 for each landmark in all three planes of space.

Table 5: Average distances and SD from T_1 to T_2 between IO-NPF, NPF-GPF and IO-GPF in all three planes of space for the right and left side

Table 6: Paired t-test for the right side comparing distances between T_1 and T_2 using the infraorbital foramen, nasopalatine foramen and the greater palatine foramen landmark

Table 7: Differences in the distance between the right and left sides of the IOF, NPF and GPF landmarks at T_1 and T_2

Tables

Table 1: Description of the sample, distribution and treatment time (N=30).

		Age at T1 (years, months)	Age at T2(years, months)	Treatment time(years, months)	Age Range
	N	Mean ± SD	Mean ± SD	Mean ± SD	
Males	14	13.57 ± 1.20	15.61 ± 1.08	2.05 ± 0.43	12.58 – 17.58
Females	16	13.51 ± 1.17	15.56 ± 1.05	2.05 ± 0.43	11.33 – 16.58
Total	30	13.56 ± 1.18	15.61 ± 1.06	2.05 ± 0.43	11.33 – 17.58

Table 2: Intraclass Correlation Coefficient of all landmarks.

Measurements	Axis	Single Measures
IOR	X	0.92
	Y	0.99
	Z	0.97
IOL	X	0.95
	y	0.99
	z	0.97
LDR	X	0.90
	y	0.97
	z	0.97
LDL	X	0.93
	y	0.98
	z	0.97
NPFR	X	0.86
	y	0.99
	z	0.99
NPFL	X	0.89
	y	0.99
	z	0.99
ANS	X	0.92
	y	0.99
	z	0.98
PNS	X	0.76
	y	0.98
	z	0.98
GPFR	X	0.83
	y	0.99
	z	0.98
GPFL	X	0.83
	y	0.98
	z	0.91

Table 3: Subject distribution according to the direction of change for all landmarks (N=30), NC= no change

	Sagittal			Axial			Coronal		
	right	left	NC	down	up	NC	Forward	back	NC
IOR	11	2	1	11	12	0	15	7	0
IOL	4	15	0	12	12	0	12	3	2
LDR	5	7	2	13	12	1	13	9	0
LDL	7	7	1	14	12	0	13	6	0
NPFR	6	11	0	16	8	1	16	2	0
NPFL	7	11	1	12	8	1	16	1	0
ANS	7	12	0	14	11	1	17	7	0
PNS	12	7	1	16	10	2	9	11	1
GPFR	12	8	3	13	7	1	13	6	1
GPFL	9	12	1	15	6	0	13	9	1

Table 4. Descriptive statistics of the absolute value of the difference between T_1 and T_2 for each landmark in all three planes of space.

Averages and SD						
	N	Sagittal	N	Axial	N	Coronal
IOR	29	0.60 ± 0.49	27	1.39 ± 1.05	29	1.10 ± 0.76
IOL	29	0.88 ± 0.62	28	1.80 ± 1.29	28	0.78 ± 0.68
LDR	28	0.53 ± 0.50	28	2.50 ± 1.83	29	1.07 ± 0.90
LDL	28	0.47 ± 0.33	29	2.77 ± 1.99	29	.094 ± 0.69
NPFR	28	0.86 ± 0.59	28	1.51 ± 0.77	24	0.77 ± 0.57
NPFL	29	0.75 ± 0.55	28	1.50 ± 1.16	29	1.19 ± 1.10
ANS	29	0.89 ± 0.71	28	1.65 ± 1.29	28	1.32 ± 0.94
PNS	28	0.66 ± 0.57	28	1.25 ± 0.74	29	0.97 ± 0.71
GPFR	29	0.87 ± 0.67	28	1.01 ± 0.85	29	0.98 ± 0.73
GPFL	29	0.95 ± 0.69	28	1.16 ± 0.89	28	0.89 ± 0.64

Table 5. Average distances and SD from T_1 to T_2 between IO-NPF, NPF-GPF and IO-GPF in all three planes of space for the right and left side *The average distance in **both** right and left sides was more than 1mm.

Axis		**Right Side**	**Left Side**
Sagittal	IO-NPF	1.05 ± 0.77	0.60 ± 0.49
	NPF-GPF	1.02 ± 0.81	0.69 ± 0.53
	IO-GPF	0.62 ± 0.53	0.81 ± 0.64
Axial	IO-NPF	0.99 ± 0.78	1.14 ± 0.90
	NPF-GPF	0.78 ± 0.62	0.83 ± 0.61
	IO-GPF	1.08 ± 0.89*	1.30 ± 1.11*
Coronal	IO-NPF	0.83 ± 0.57	0.78 ± 0.73
	NPF-GPF	0.90 ± 0 .74	1.27 ± 1.16
	IO-GPF	0.71 ± 0.41	0.92 ± 0.84

Table 6. Paired t-test for the right side comparing distances between T_1 and T_2 using the infraorbital foramen, nasopalatine foramen and the greater palatine foramen landmarks (N=30). *Significant at $p \leq 0.05$ using paired t-test.

		Paired Differences Left side		Sig. (2-tailed)	Paired Differences Right side		Sig. (2-tailed)
		Mean	Std. Deviation	P-value	Mean	Std. Deviation	P-value
Pair 1	T1IOx_NPFRx - T2IOx_NPFx	.80	1.03	.000*	-.40	.67	.002*
Pair 2	T1NPFx_GPFx - T2NPFx_GPFx	-.50	1.21	.031*	-.02	.87	.86
Pair 3	T1IOx_GPFx - T2IOx_GPFx	.30	.76	.038*	-.43	.94	.01*
Pair 4	T1IOy_NPFy - T2IOy_NPFy	-.74	1.02	.000*	-.92	1.13	.000*
Pair 5	T1NPFy_GPFy - T2NPFy_GPFy	.00	1.01	.99	-.17	1.02	.36
Pair 6	T1IOy_GPFy - T2IOy_GPFy	-.73	1.20	.002*	-1.09	1.31	.000*
Pair 7	T1IOz_NPFz - T2IOz_NPFz	.39	.94	.031*	.32	1.02	.09
Pair 8	T1NPFz_GPFz - T2NPFz_GPFz	-.70	.93	.000*	-.74	1.55	.01*
Pair 9	T1IOz_GPFz - T2IOz_GPFz	-.31	.76	.034*	-.42	1.18	.06

Table 7. Differences in the distance between the right and left sides of the IOF, NPF and GPF landmarks at T_1 and T_2

*Significant at $p \leq 0.05$ using paired t-test.

		Paired Differences		Sig. (2-tailed)
		Mean	Std. Deviation	P value
Pair 1	T2IORxIOLx - T1IORxIOLx	-1.04	± 0.98	.00*
Pair 2	T2IORyIOLy - T1IORyIOLy	-0.18	± 0.89	.26
Pair 3	T2IORzIOLz - T1IORzIOLz	-0.06	± 1.01	.74
Pair 4	T2NPFRxNPFLx - T1NPFRxNPFLx	0.20	± 0.66	.10
Pair 5	T2NPFRyNPFLy - T1NPFRyNPFLy	-0.003	± 0.09	.83
Pair 6	T2NPFRzNPFLz - T1NPFRzNPFLz	0.01	± 0.05	.32
Pair 7	T2GPFRxGPFLx - T1GPFRxGPFLx	-0.34	± 0.82	.03
Pair 8	T2GPFRyGPFLy - T1GPFRyGPFLy	0.16	± 0.71	.22
Pair 9	T2GPFRzGPFLz - T1GPFRzGPFLz	0.02	± 1.20	.92

C. Figures representing landmark location:

Figure 1. Location of the Infraorbital Foramen

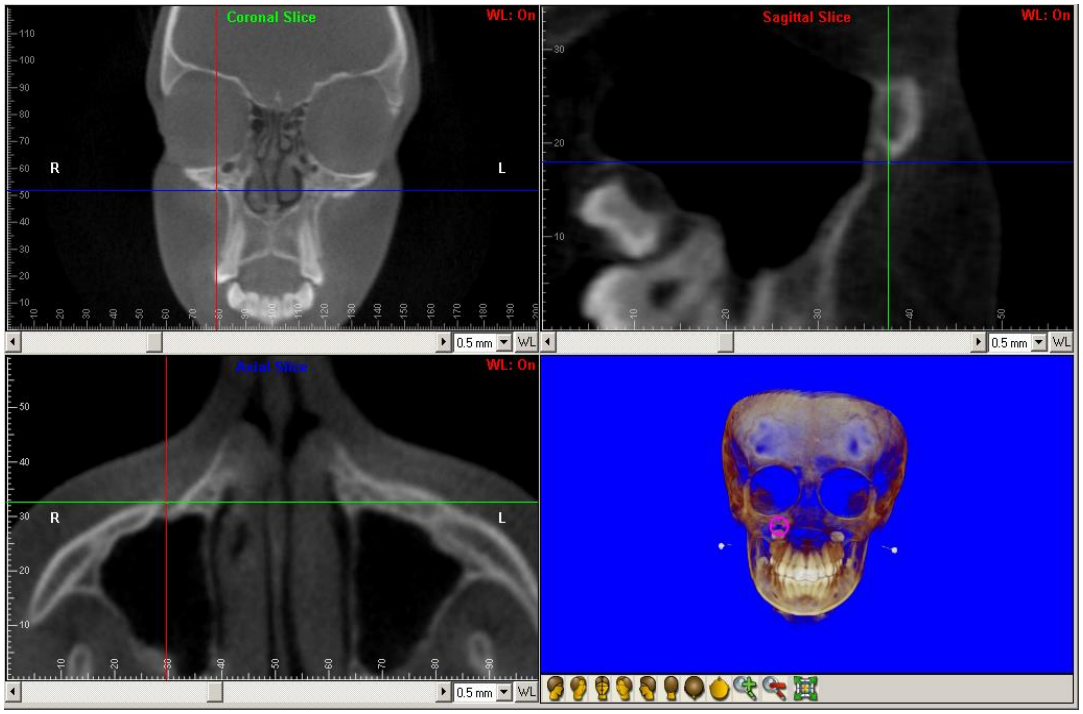


Figure 2. Lacrimal Duct. A) Lacrimal right and left radiopacity (RO) in the coronal slice, tilting the head so that the axial refence line passes through the center of both RO. B) Visualizing the right RO in the sagittal slice and placing the landmark in the highest point of the RO. C) The volume was set and with the symmetry caliper set in the horizontal plane, the landmark was placed upon the horizontal reference line until the first contact with the frontal process of the maxilla.

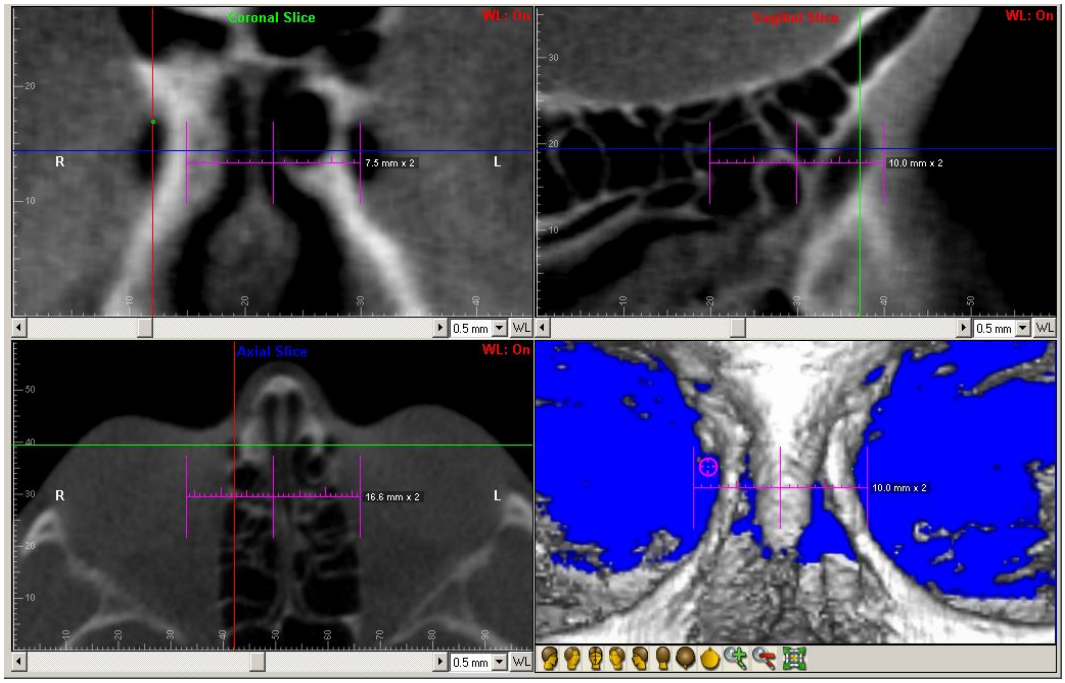


Figure 3. Nasopalatine Formane. The most posterior part of the foramen as seen in the sagittal view was located first and the axial reference line was placed on that mark, then in the axial slice, the sagittal and coronal reference lines were located in the center of the foramen, this allowed a clear view of the canal on the coronal slice. Both landmarks were placed on the axial reference line when in contact to the inner cortical surface of the canal on the coronal slice.

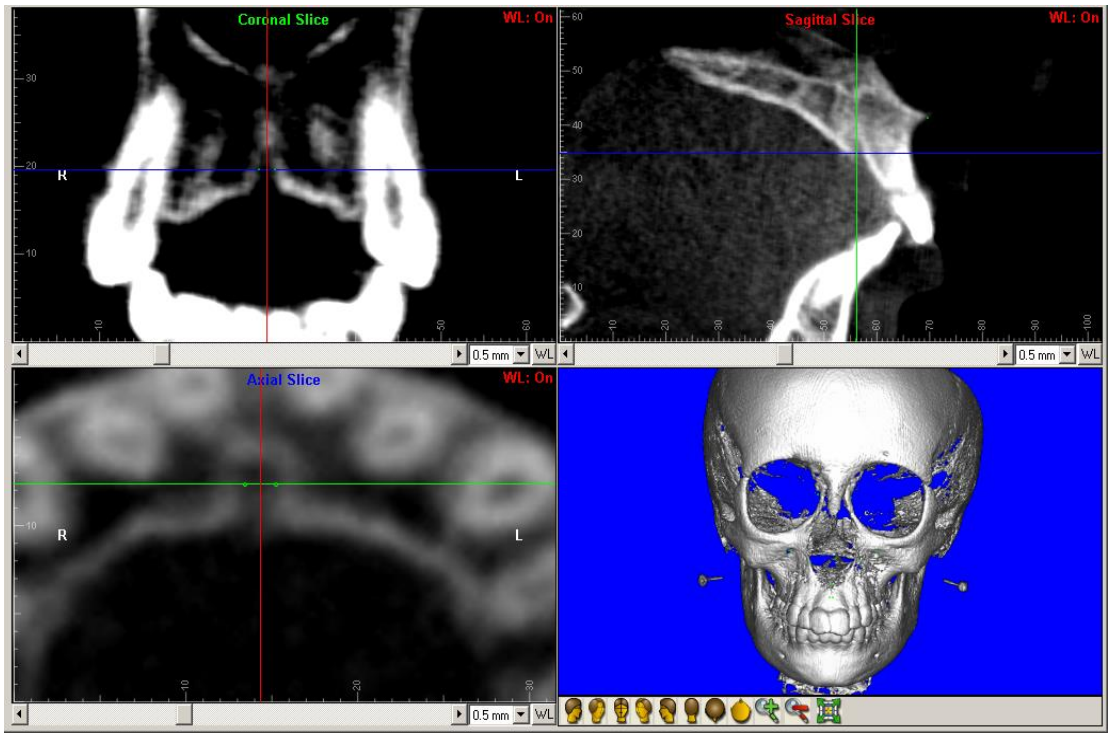


Figure 4. Anterior nasal spine (ANS). Considered as the junction of the right and left side, because of the difficulty to place 2 landmarks in that area, we considered ANS as the most anterior part where the right and left maxilla meet.

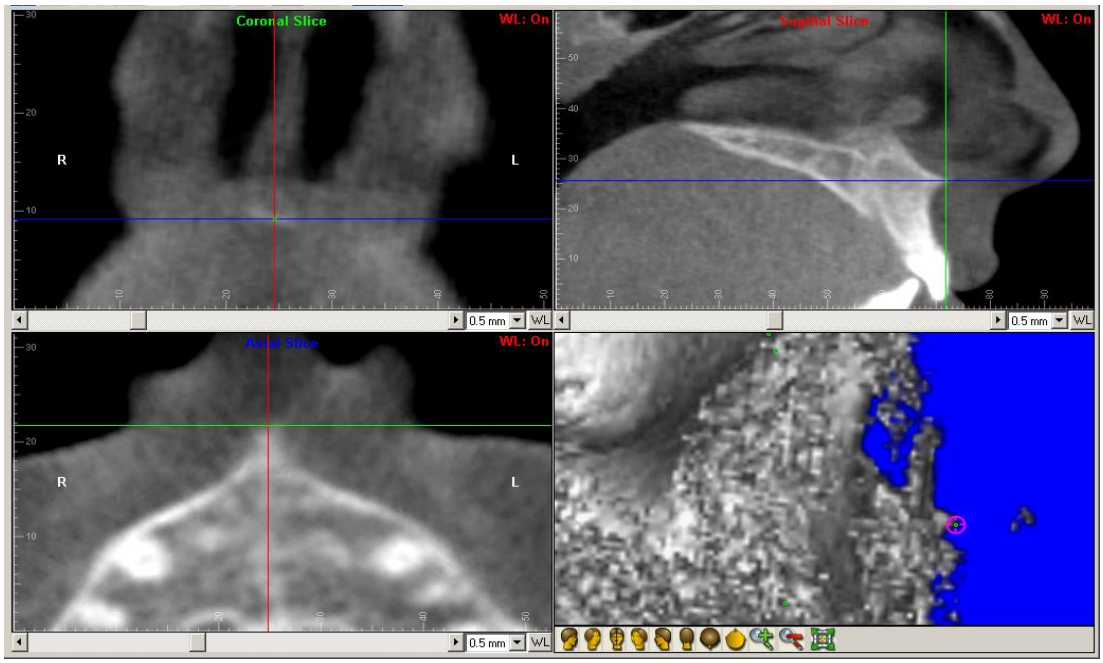


Figure 5. Posterior nasal spine (PNS). Considered as the junction of the right and left palatine bone, because of the difficulty to place 2 landmarks in this area, we considered PNS the most posterior part where the right and left palatal bones meet.

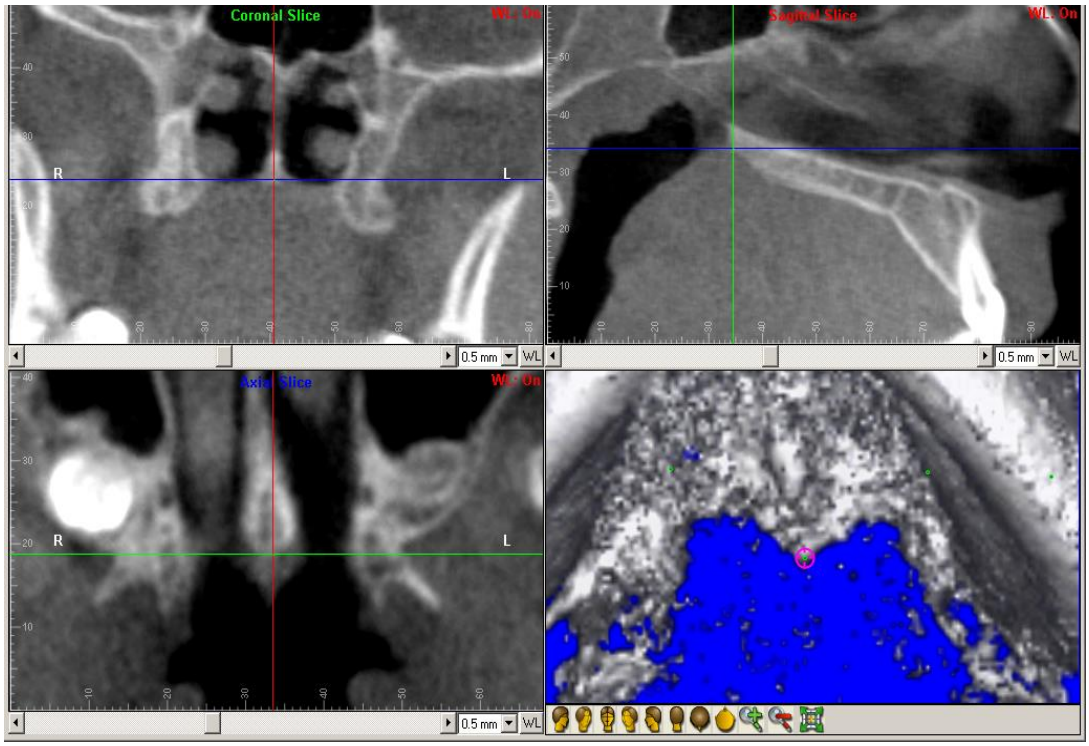


Figure 6. Greater Palatine Foramen (GPF). Location in the coronal slice. The coronal line was scrolled from inferior to superior until a clear outline of the foramen was first seen on both sides in the axial plane. Rotation of head to align the center of both foramina. Then the tilting of the head is then made to line the horizontal line with the floor of the nose in the coronal plane.

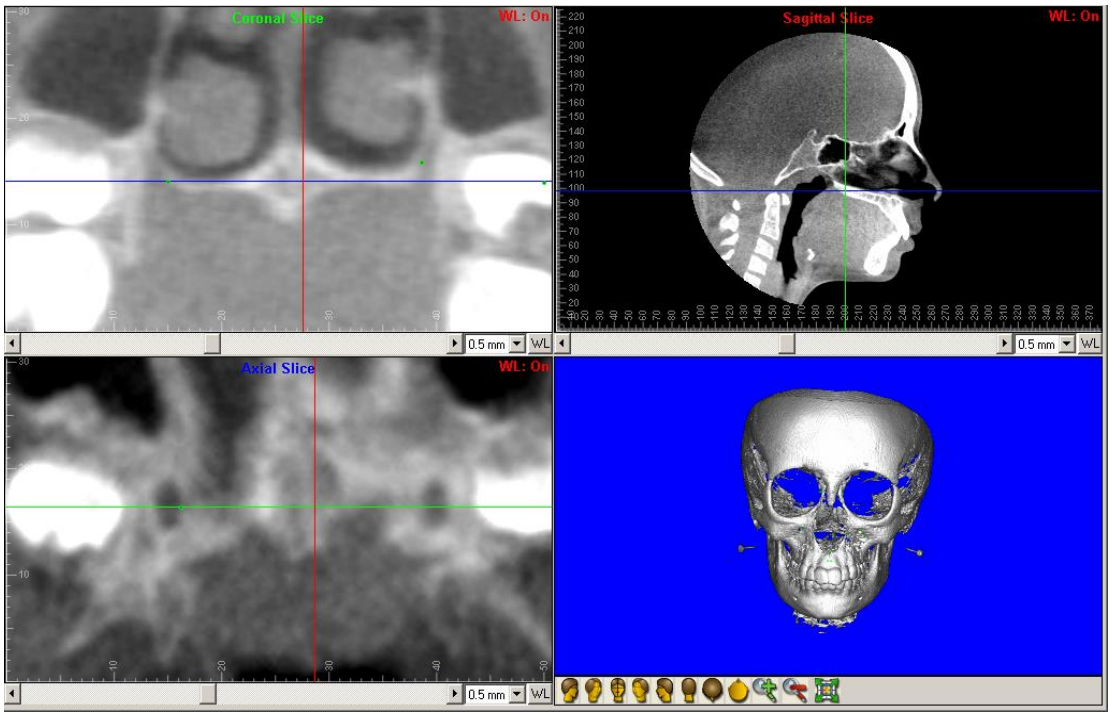
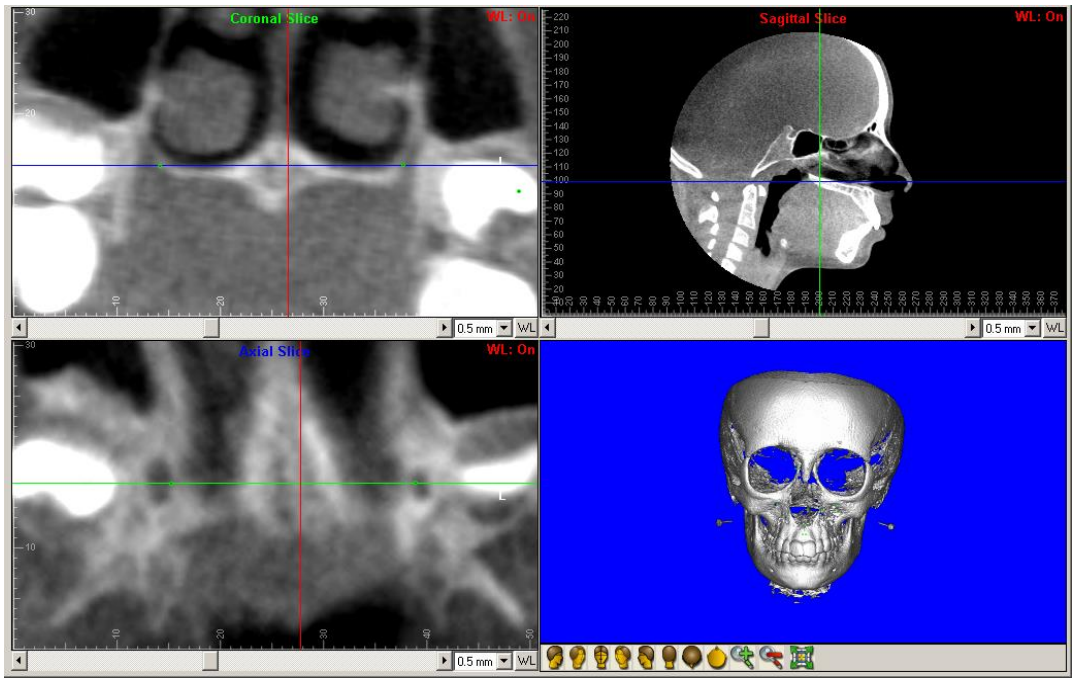


Figure 7. Greater Palatine Foramen (GPF). After orientation (see Figure 6), landmarks were placed in the coronal slice across the horizontal line when in contact with the most medial point of the canal.The axial view confirms the landmarks are seen in the outer border of the foramen.



D. **Figures representing orientation method**:

Figure 8. Coronal view, the axial plane was aligned with the center of the left and right optical foramina by tilting the head.

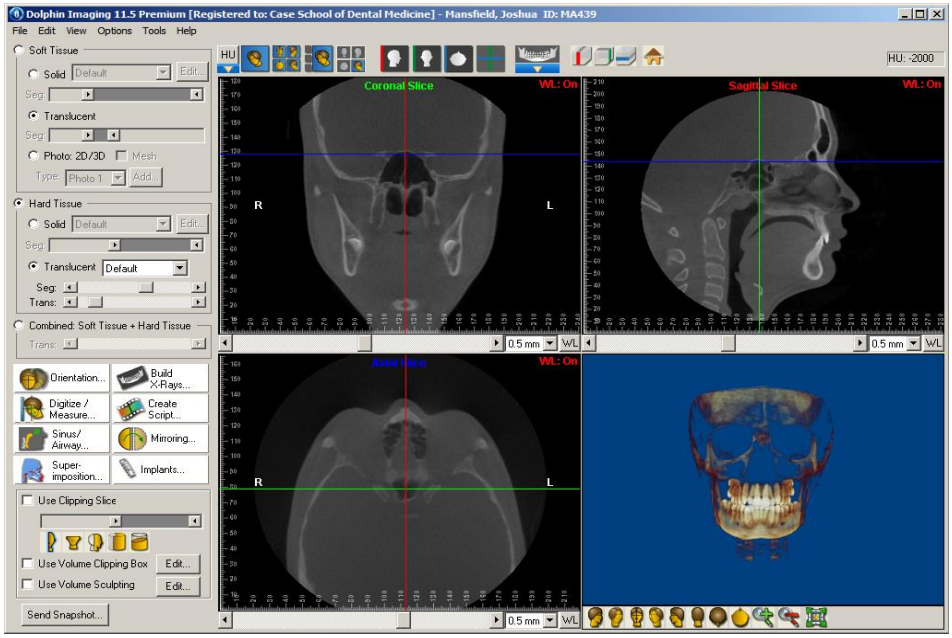


Figure 9. In the axial view the coronal plane will be aligned with the center of the left and right foramina ovale by rotating the head.

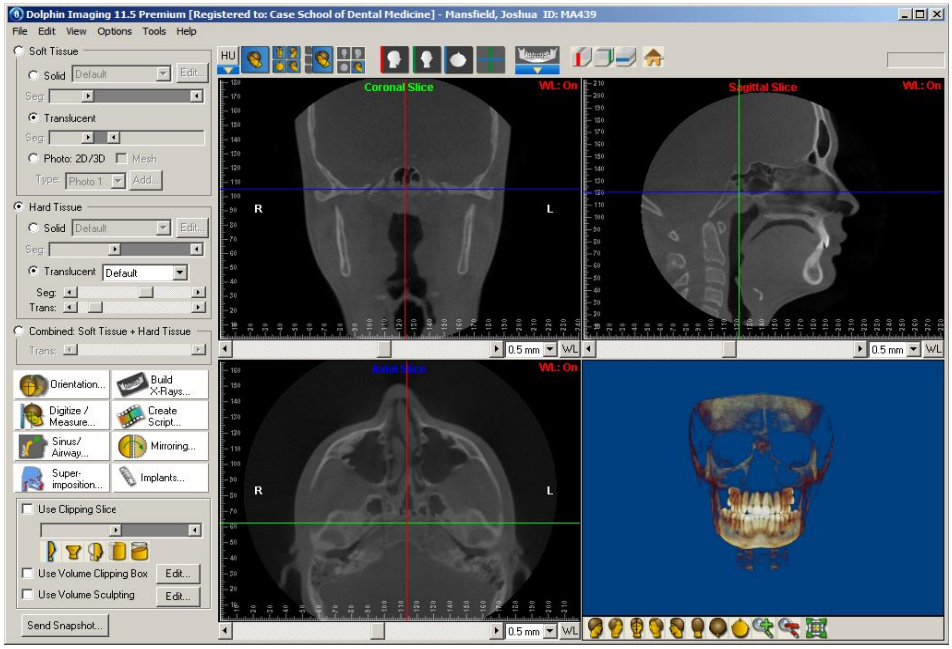


Figure 10. The axial plane was scrolled to until the foramen cecum was seen.

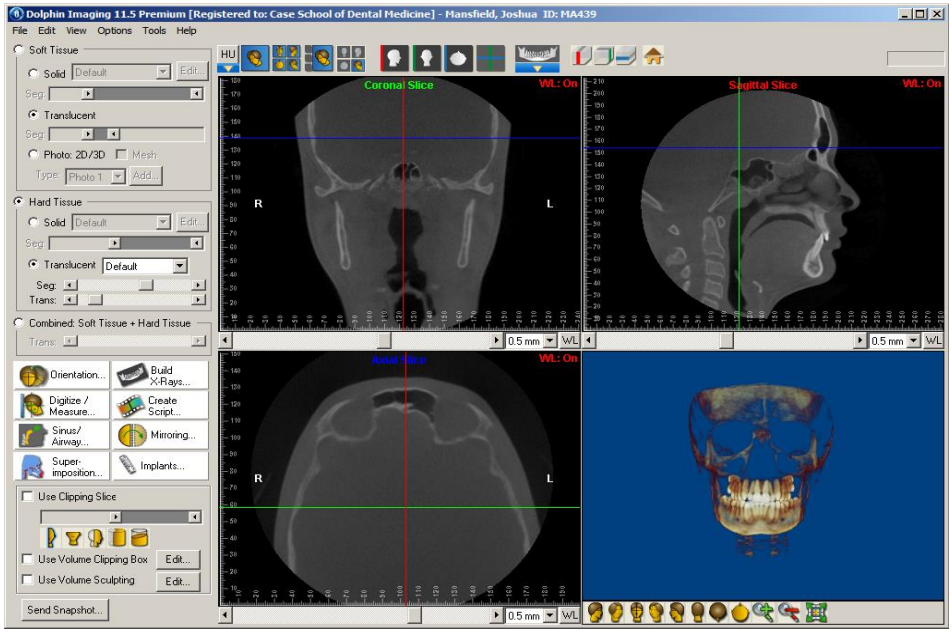
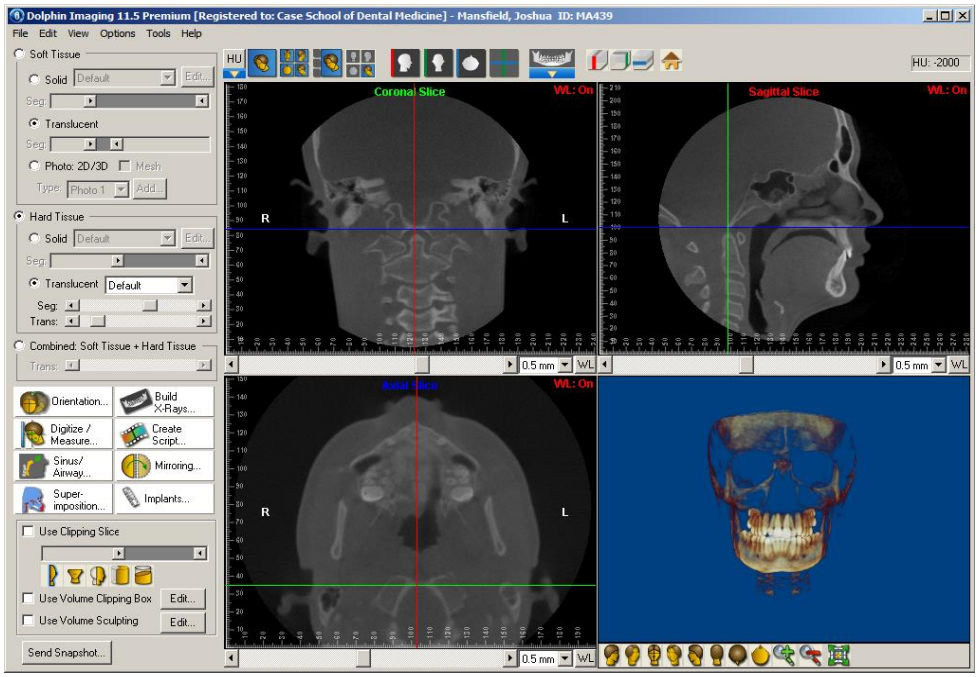


Figure 11. The sagittal plane will be positioned to pass through foramen cecum. In the sagittal view, the pitch of the head will be adjusted so that the axial plane overlapped McRae's line (Basion to Opisthion).



E. Envelope of Error Scattergrams of all 60 volumes (T1 and T2):

Figure 12. Scatter grams showing the distribution of the estimated errors of the Infraorbital Foramen landmarks of the right and left side in the three planes of space. A total of 60 scatter plots were used (T1 and T2).

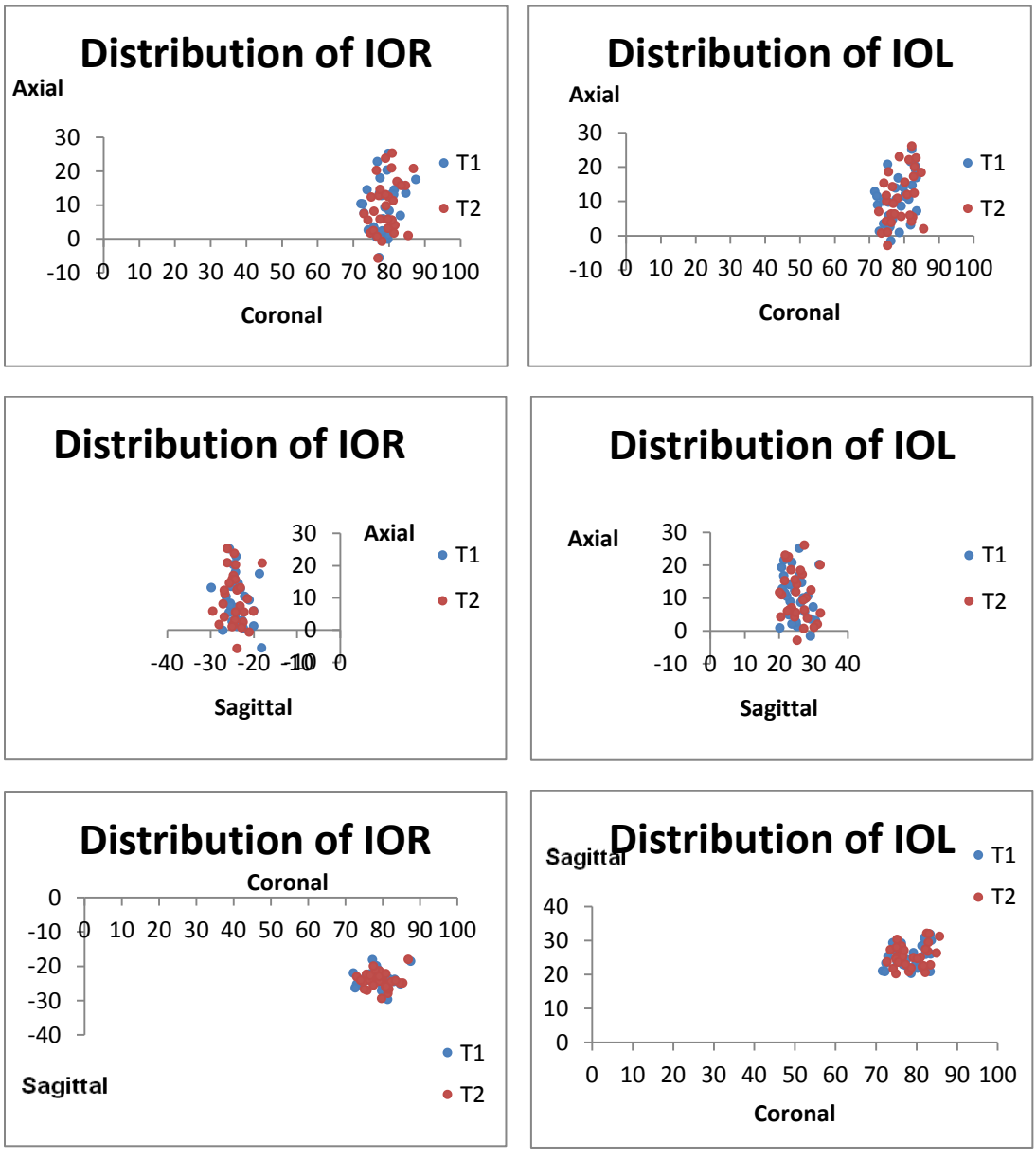


Figure 13. Scatter grams showing the distribution of the estimated errors of the Lacrimal Duct landmarks of the right and left side in the three planes of space. A total of 60 scatter plots were used (T1 and T2).

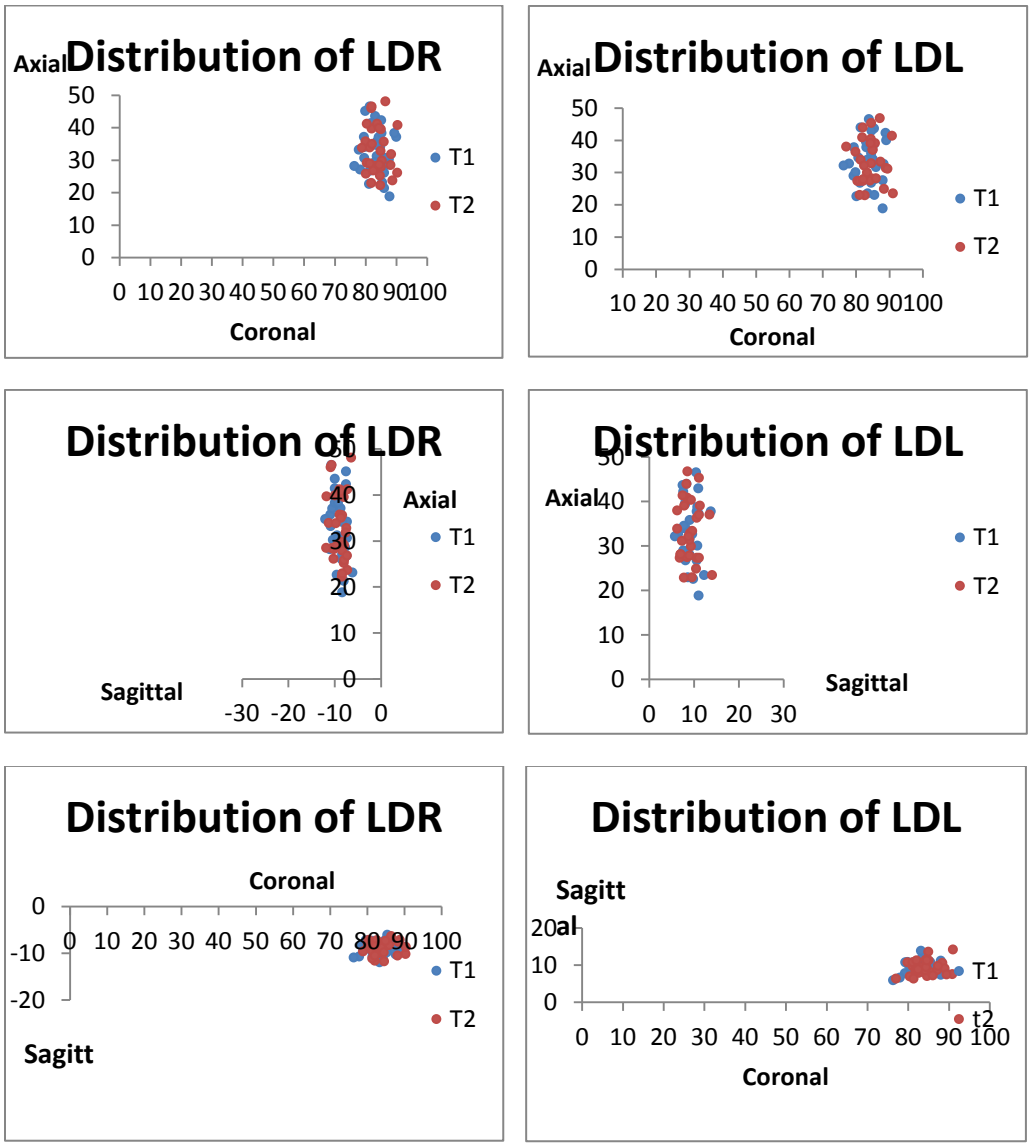


Figure 14. Scatter grams showing the distribution of the estimated errors of the Nasopalatine Foramen landmarks of the right and left side in the three planes of space. A total of 60 scatter plots were used (T1 and T2).

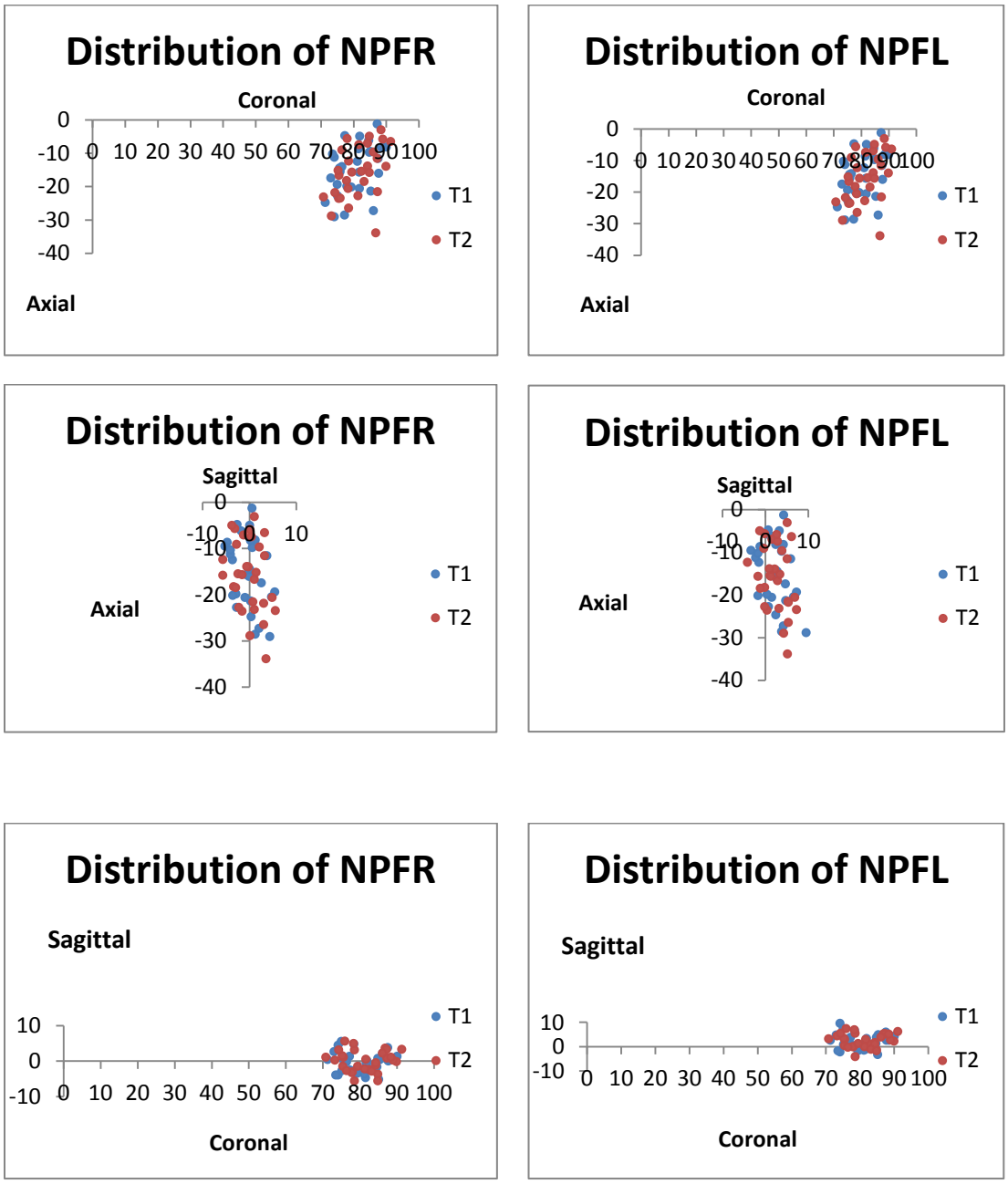


Figure 15. Scatter grams showing the distribution of the estimated errors of ANS and PNS in the three planes of space. Note that the envelope of error is similar in both ANS and PNS. A total of 60 scatter plots were used (T1 and T2).

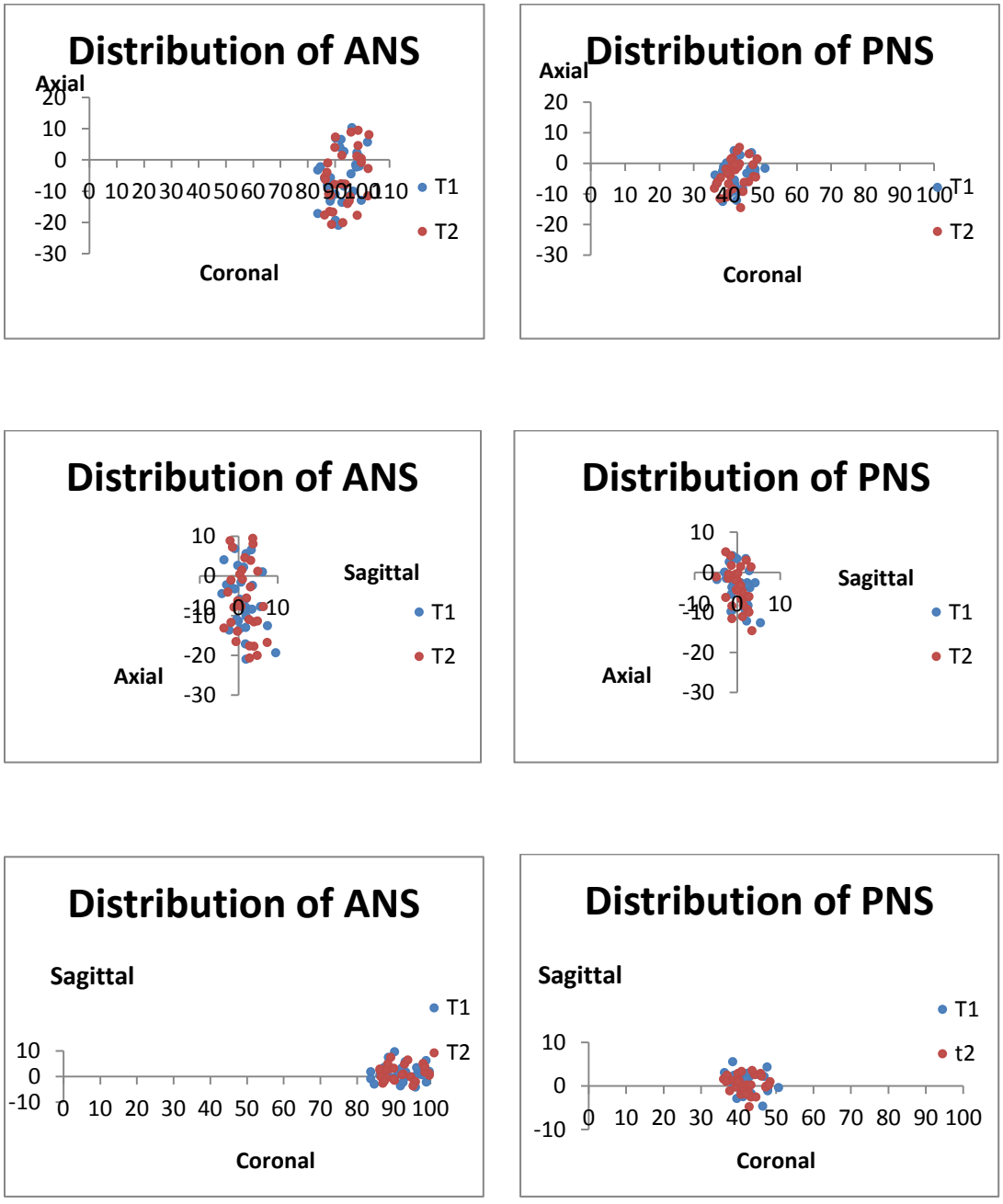
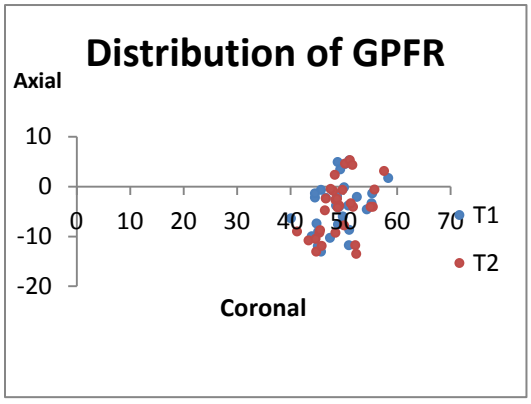
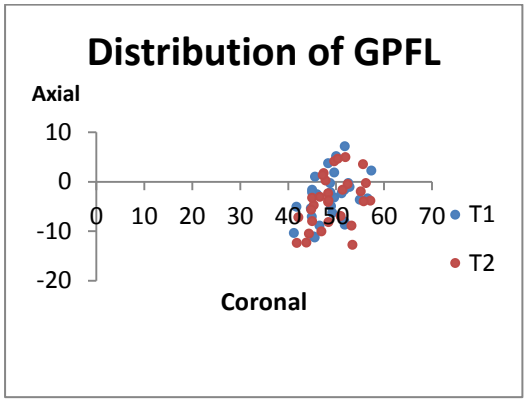
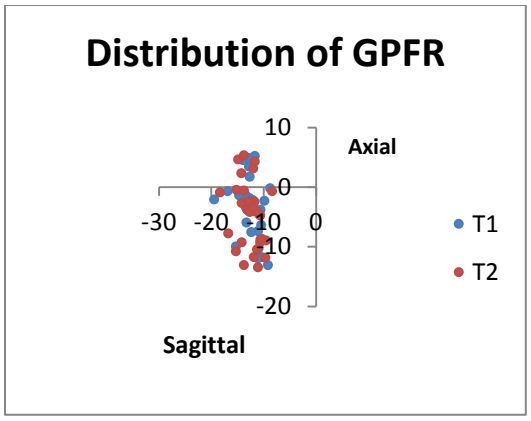
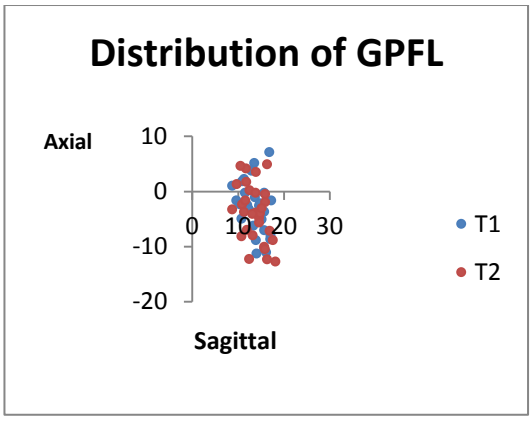


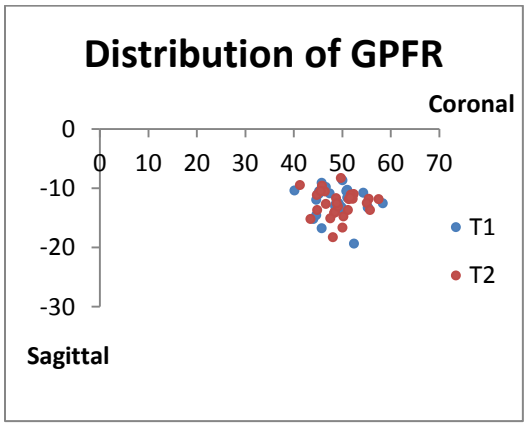
Figure 16. Scatter grams showing the distribution of the estimated errors of the Greater Palatine Foramen landmarks of the right and left side in the three planes of space. A total of 60 scatter plots were used (T1 and T2).

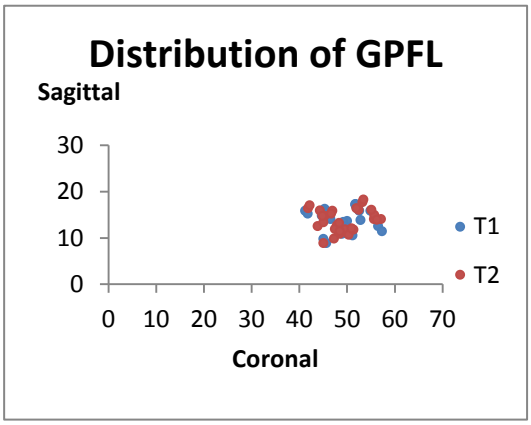












F. Reliability Scattergrams:

Figure 17. Scatter grams showing reliability and the distribution of the estimated errors of the IO landmarks of the right and left side in the three planes of space. A total of 20 volumes were used and replotted three times, therefore a total of 60 plots were used in each graph.

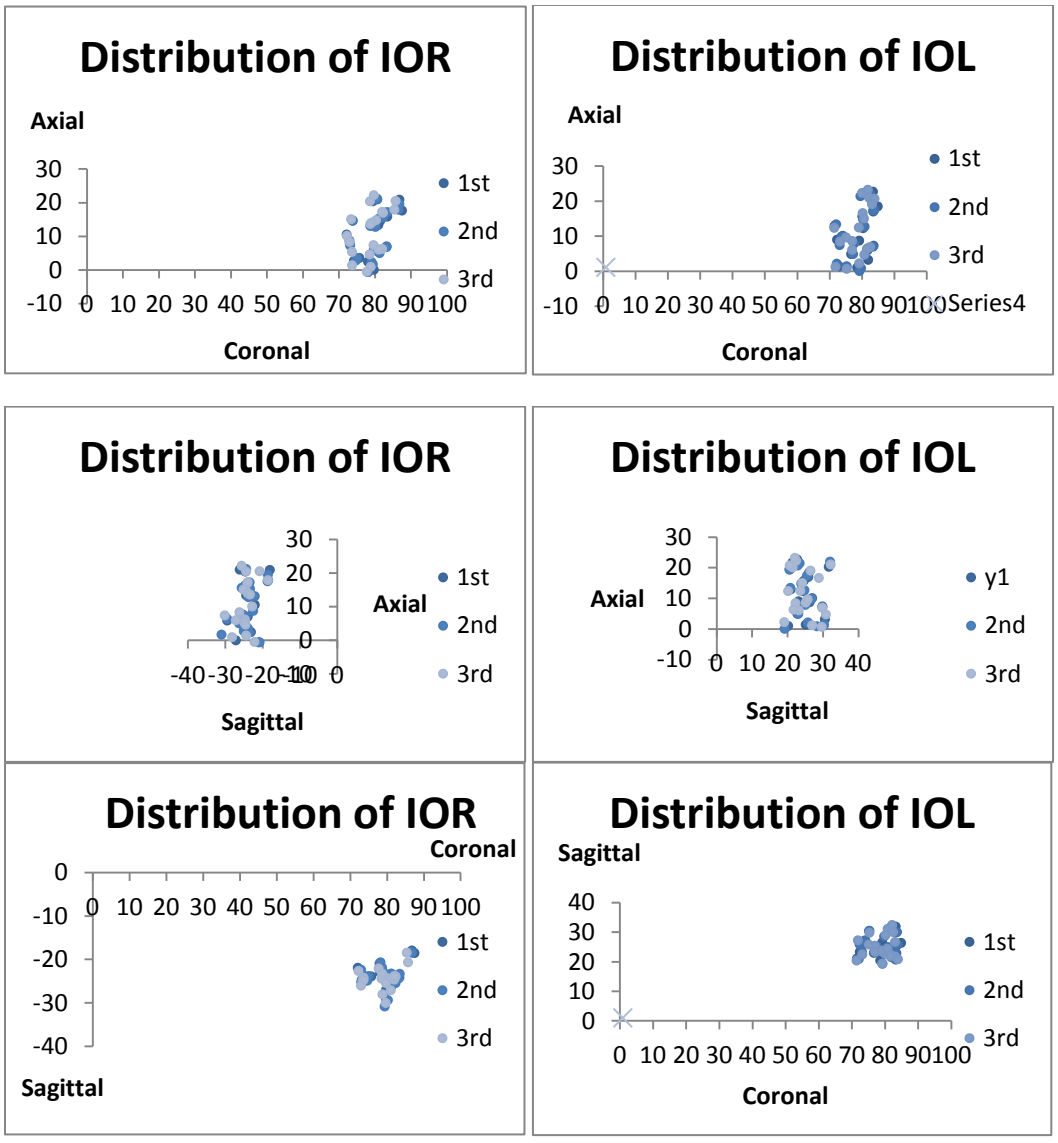


Figure 18. Scatter grams showing reliability and the distribution of the estimated errors of the LD landmarks of the right and left side in the three planes of space. A total of 20 volumes were used and replotted three times, therefore a total of 60 plots were used in each graph.

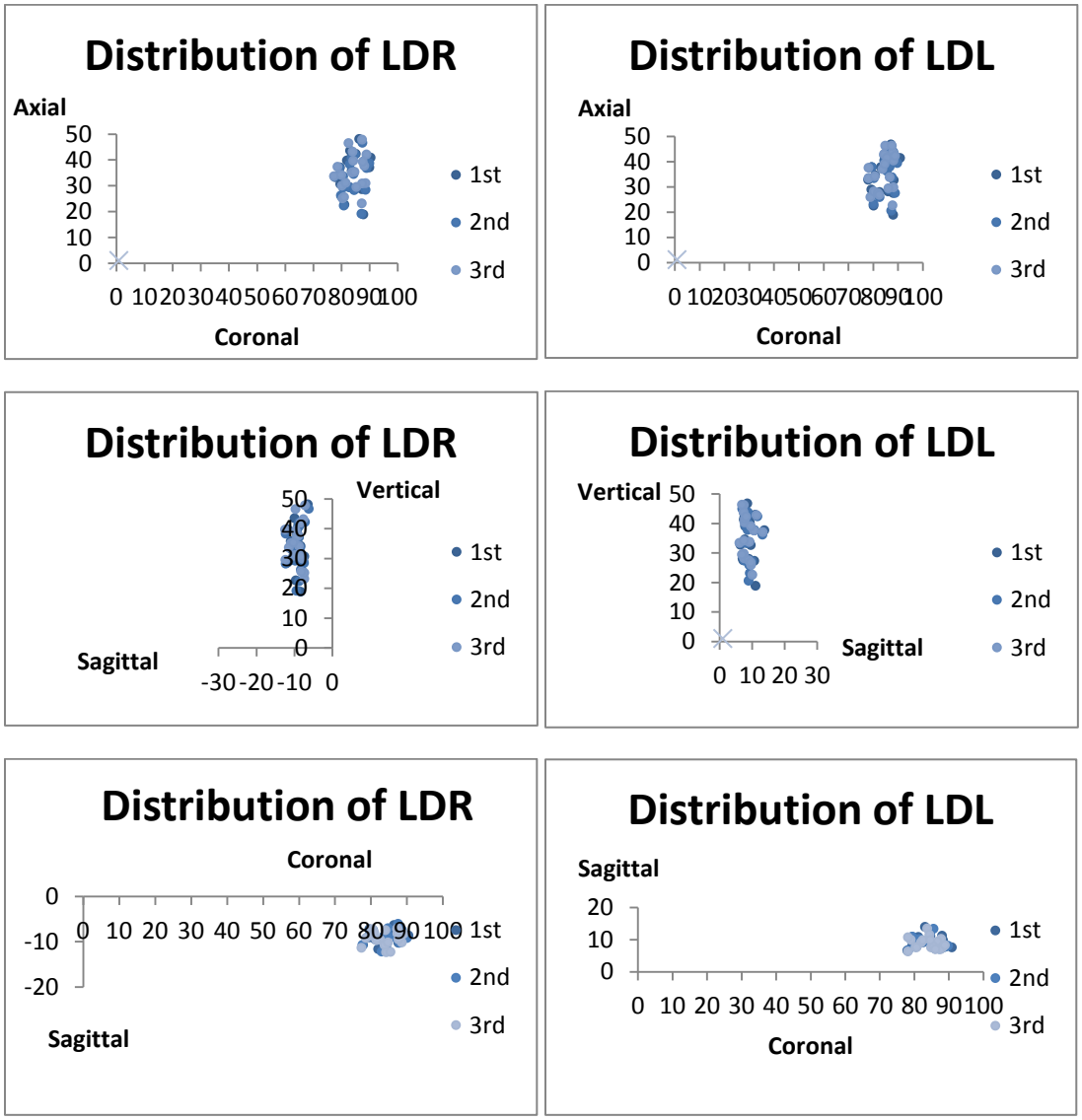
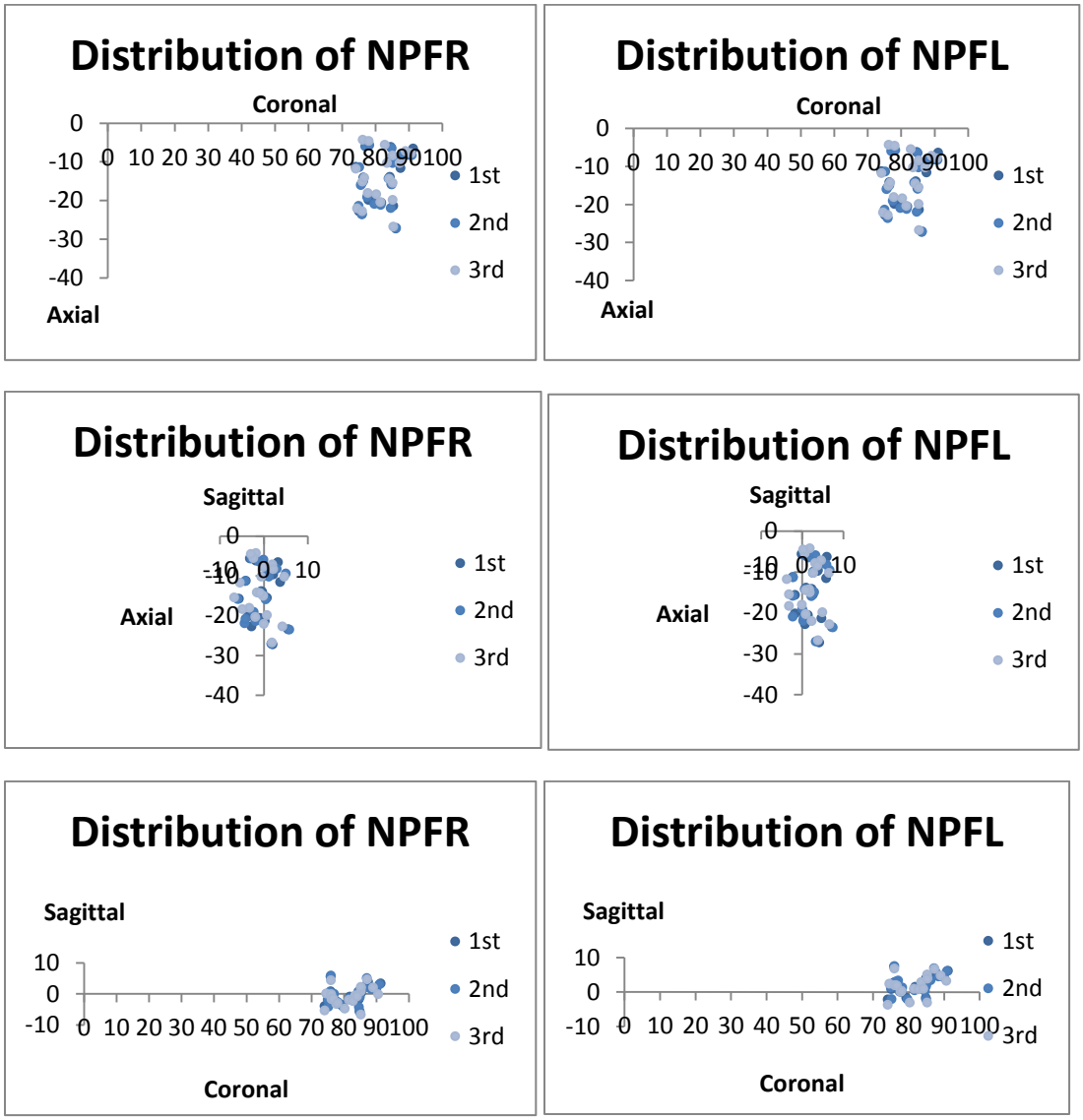


Figure 19. Scatter grams showing the distribution of the estimated errors of the NPF landmarks of the right and left side in the three planes of space. The sagittal plane is the most variable plane. A total of 20 volumes were used and replotted three times, therefore a total of 60 plots were used in each graph.



.

Figure 20. Scatter grams showing the distribution of the estimated errors of the Anterior and Posterior Nasal Spine in the three planes of space. Note that the envelope of error is similar in both ANS and PNS. A total of 20 volumes were used and replotted three times, therefore a total of 60 plots were used in each graph.

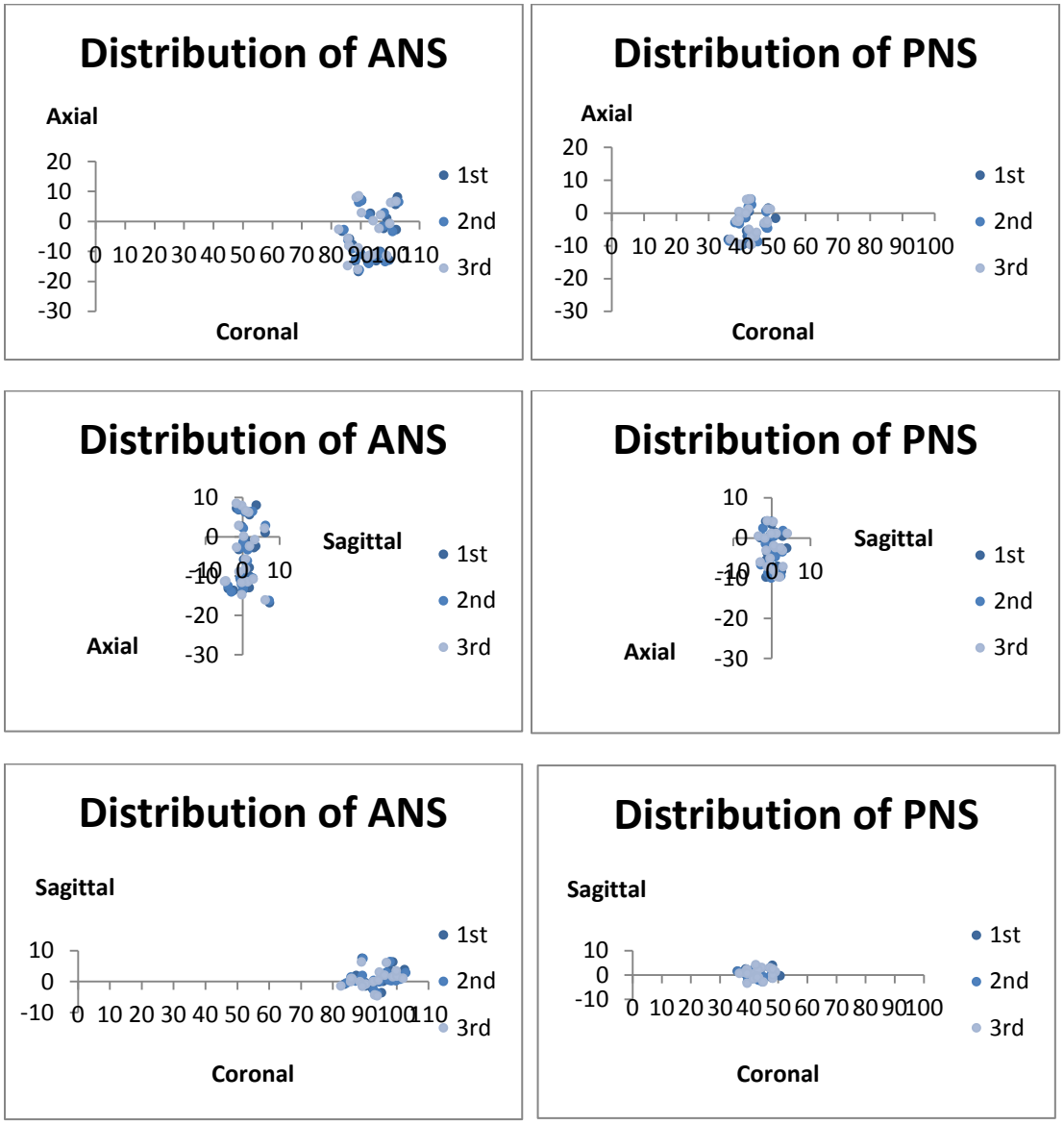
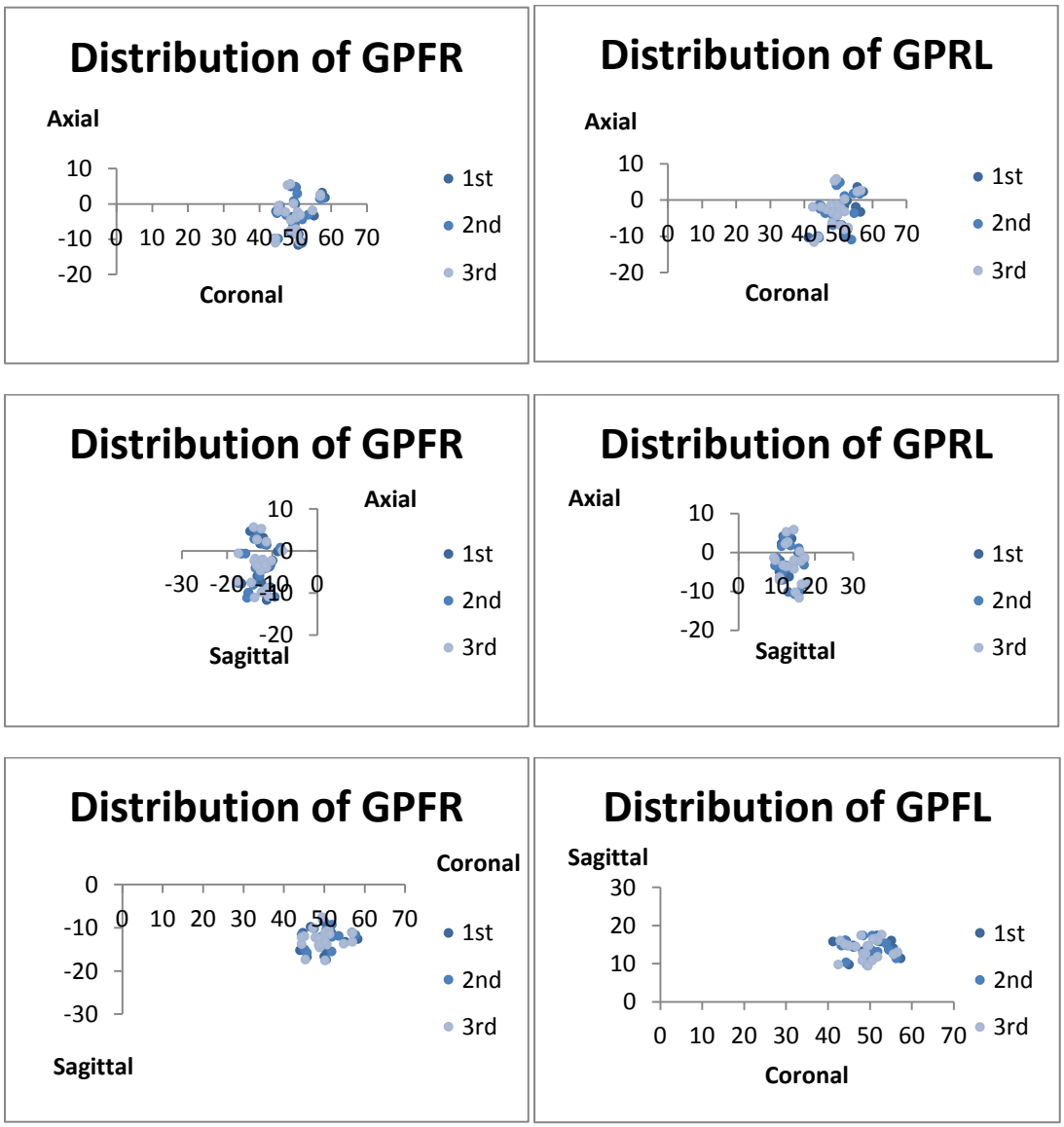


Figure 21. Scatter grams showing the distribution of the estimated errors of the Greater Palatine Foramen Landmarks of the right and left side in the three planes of space. Similar envelopes of error are seen on the right and left side. Dispersion in the sagittal axis seems the largest, but it follows a circular envelope of error. A total of 20 volumes were used and replotted three times, therefore a total of 60 plots were used in each graph.



G. RAW DATA

Raw data from T_1 of all subjects.

	IOR	IOL	LDR	LDL	NPFR	NPFL	ANS	PNS	GPFR	GPFL
BR245	-24.3	24.6	-9.1	10.7	-1.7	1.2	-0.1	-1.2	-13.3	12.5
BR245	13.3	12.2	37.1	37.7	-6.2	-6.2	2.6	-3.7	-3.4	-3.4
BR245	81	80.5	79.6	79.4	84.7	84.7	93.4	47.9	55.3	56.6
CA266	-27.1	30.7	-8.3	11.1	0.3	4.8	1.9	2.6	-11.1	17.4
CA266	-0.1	3.1	18.8	18.8	-21.4	-21.4	-13	-8.3	-11.7	-8.3
CA266	79.8	82	87.9	88.1	85.4	85.4	99.8	44.3	50.9	52.7
CO334	-18.1	29.2	-6.1	12.3	4.4	9.5	9.6	5.5	-9.1	16.2
CO334	-5.6	-1.6	23.1	23.4	-29.1	-28.9	-19.4	-12.6	-13.1	-11.1
CO334	77.3	76.3	85.5	83.6	74.2	74.2	90.3	38.5	45.8	45.4
CR96	-24.9	25.3	-9.5	9.9	-2.7	0	0.5	-1.4	-15.2	15.8
CR96	2.6	1.3	22.6	22.5	-22.8	-22.8	-13.3	-9.8	-10	-10.4
CR96	74.3	73	81.2	80.2	75.2	75.2	88.3	40.7	44.1	41.3
DO111	-23.8	25.1	-8.5	9	1.3	3.8	2	2.3	-11	14.1
DO111	1.1	2.6	26.1	27.9	-28.6	-28.6	-21	-12.2	-12	-11.3
DO111	79.9	76	86.1	85.9	77.3	77.3	91.4	42.5	45.2	45.6
GR221	-22	23.3	-7.3	7.7	0.8	2.7	1.9	2.4	-9.8	14.7
GR221	10.4	8.9	30.6	28.9	-15.6	-15.6	-7.9	-2.6	-2.3	-2.6
GR221	72.2	72.5	79.7	79.3	76	76	87.4	38.9	46.7	46.1
GR223	-21	22.3	-8.2	8.2	-0.6	2.3	1.7	-1.1	-13	12.1
GR223	9.3	10.5	28.4	26.7	-15.7	-15.7	-8.5	-2	-3.8	-2.5
GR223	78.9	77.8	85.4	84.6	81.8	81.8	93.4	41.2	48.6	48.6
HE140	-24.6	21.5	-9.9	7.5	-2.6	0.7	-0.9	0	-12.7	13.6
HE140	20.3	21.6	43.5	43.6	-4.8	-4.8	6.8	3.4	4.9	5.1
HE140	79.5	82	83.2	85.5	77.4	77.4	90.4	42.8	48.9	50.1
HI91	-23.5	24.4	-9.4	8.3	0.1	2.8	2	-0.1	-12.6	11.6
HI91	13.4	13.9	31.2	33.8	-14.5	-14.5	-5.8	-2.9	-1.9	-0.3
HI91	77.4	77.6	83.7	83.5	75.8	75.8	88.4	39.8	48.8	48.8
JA141	-23.9	30	-10.9	13.8	2.1	4.2	2	2	-10.3	17.2
JA141	6.9	7.2	35.7	37.7	-27.3	-27.3	-10.1	-9.5	-8.7	-8.1
JA141	83.3	83.7	83.8	83.2	86.2	86.2	96.7	42.9	51.1	51.8
KE115	-22.3	23.8	-8	8.7	0.4	2.5	1.8	2.2	-10.9	14
KE115	0.5	2.1	21.3	22.9	-24.8	-24.7	-17.2	-7.2	-10.3	-8.9
KE115	76.6	75.7	86.1	85.6	71.4	71.4	83.8	41.8	47.5	46.6
KL48	-18.6	20.8	-8.7	7.7	1.3	4.2	2	-0.4	-12.6	11.4
KL48	17.5	19.3	37.1	42.2	-8.2	-8.2	5.6	-1.7	1.7	2.2

KL48	87.6	83.4	90.1	88.9	90.1	90.1	102	50.8	58.4	57.4
KU46	-24	23.8	-7.5	8.4	0.1	3.3	3.3	-1	-13.9	13
KU46	22.8	20.8	45.1	43.9	-5	-5	6.5	4.1	4.5	3.7
KU46	76.8	75.3	80	81.4	82	82	92.3	41.8	50.3	48.4
LA146	-24.5	31.8	-7.5	11	3.8	5.9	6.2	2.9	-8.7	15.8
LA146	16.3	20.2	42.3	42.9	-11.6	-11.6	1	0.4	-0.2	-0.3
LA146	83	83.4	85.2	84.7	87.6	87.6	98.9	42.6	50.1	52.6
LO74	-24.1	21.4	-9.9	8.1	-4.7	-1.2	-3.7	-1.8	-12.7	11
LO74	18	16.8	41.4	39.4	-8.7	-8.7	4	2.6	3.4	1.8
LO74	77.6	78.4	81.9	83.1	81.6	81.6	91.9	43.5	49.4	49.7
MI228	-19.9	29.3	-8.3	10.8	5.5	7.3	7.5	2.1	-11	15.8
MI228	1.2	3.5	27.1	30	-19.4	-19.4	-12.6	-6.6	-7.4	-7.1
MI228	77.7	74.2	78.3	79.9	75.1	75.1	88.6	36.8	45	45
OR26	-25.6	26.4	-10.3	9.7	-0.9	1.5	0	1.5	-12.3	13.4
OR26	5.4	8.6	30.2	32.6	-20.6	-20.6	-11.4	-7.1	-7.6	-6.3
OR26	80.9	79.3	87.7	88.4	81.9	81.9	95.8	42.1	49	49.3
RA98	-22.6	27.5	-7.4	10.7	2.6	4.7	3.5	3	-10.4	15.2
RA98	2.9	5.8	26.7	26.7	-17.5	-17.5	-8.4	-3.9	-6.4	-5.1
RA98	75.9	75.6	81.5	81.3	73.1	73.1	87.5	36.3	40.2	41.8
RO260	-25.3	28.4	-9.3	9.1	0	2.6	0.7	2.5	-10.8	15.8
RO260	8.3	10.6	30.6	31.6	-16.1	-16.1	-1.6	-3.3	-4.6	-3.7
RO260	80.1	81.4	86.6	86.1	87.8	87.8	97.7	45.5	54.4	55
SE83	-19.9	27.6	-7.3	11.1	4.8	6.6	5.7	1.9	-10.5	14.8
SE83	5.9	9.7	34.2	37.2	-20.5	-20.5	-7.8	-6.8	-9.1	-5.4
SE83	78.4	75.6	84.9	84.7	78.5	78.5	93.2	36.8	45.3	44.8
ST234	-23	23.1	-10.5	9.1	-3.6	-1.5	-2.2	-0.3	-13.4	12.4
ST234	12.8	14.1	37	35.8	-12.5	-12.4	-2.1	-1.2	-2.5	-3.2
ST234	78	79.9	84.4	84.6	81.2	81.2	99	38.7	48.7	49.7
TO91	-25.2	26.6	-9.9	10.8	0.3	2.5	1.4	-0.6	-13.3	13.8
TO91	13.5	14.7	38.3	38.7	-8.3	-8.2	2.2	-2	-1.4	-1.1
TO91	84.8	82.4	85.3	85.5	88.6	88.6	98.1	47.9	55.4	52.9
WA203	-23.5	26	-9.2	8.2	0.7	3.8	3.6	3.9	-10.5	17.3
WA203	14.5	16.9	38.3	39.9	-9.8	-9.8	-2.4	-2.6	-3.8	-1.7
WA203	81.6	83.6	89.5	89.1	84.9	84.9	97.9	47.7	50.9	51.8
WH73	-23.9	21	-10.8	6.5	-4	-2.2	-0.9	-2.9	-16.8	9.7
WH73	14.5	12.8	33.2	32.7	-11.3	-11.3	-3.3	0	-0.7	-1.7
WH73	73.9	71.7	77.9	78	74.2	74.2	83.8	39.6	45.8	45.1
YO39	-24	22.9	-9.8	9.1	-2.8	0.4	-0.4	-1.3	-13.2	10.8
YO39	3.5	4.8	29.3	27.9	-19.9	-19.9	-11	-5.5	-6	-5
YO39	75.8	76.8	83.1	82.6	78	78	90.2	41.9	49.9	49
CA235	-23	20.3	-7.7	7.3	-3.5	-1.7	-2.3	-0.3	-12.5	11

CA235	2.3	0.9	28.6	27.5	-20.2	-20.2	-13.7	-1.5	-4	-2.2
CA235	78.2	78.7	87.4	88.1	79.4	79.4	92.6	41.6	49.2	48.9
GR205	-29.7	21.8	-12	7.7	-5.2	-3.3	-4.2	-4.7	-19.4	10.5
GR205	13.1	11.5	34.7	34	-9.5	-9.6	-4.5	-1.8	-2.1	-2.4
GR205	81.4	80.3	83.4	85.1	85.2	85.2	96	46.5	52.5	51.2
MO234	-25.3	27.1	-8.3	7.8	-0.3	2.4	0.4	0.9	-12	14.9
MO234	7.6	10	34.1	34.5	-14.1	-14.2	-5.9	-2.6	-2.2	-2.2
MO234	73.1	74.2	80	80.8	76.5	76.5	86.3	38.5	44.7	45.1
SC181	-26.3	20.8	-11	5.8	-4	-1.7	-3	-2.5	-14.6	8.8
SC181	10.3	11.5	28.2	32.1	-10.3	-10.3	-2.3	-1.5	-1.4	1
SC181	72.7	72.3	76.4	76.4	73.6	73.6	84.8	41.3	44.7	45.7
SC177	-25.5	25.9	-10.7	10.5	0.6	4.3	3.4	2.1	-11.6	16.9
SC177	25.2	25.2	46.5	46.5	-1.3	-1.3	10.2	3.4	5.2	7.1
SC177	79.9	82.3	81.5	83.9	87.3	87.3	96.3	46.9	51.1	51.9

Raw data from T_2 from all subjects.

IOR	IOL	LDR	LDL	NPFR	NPFL	ANS	PNS	GPFR	GPFL
-23.8	25	-8.9	10.7	-1.2	1.6	0.9	-0.1	-11.8	14
12.4	11.9	35.7	36.3	-7.1	-7	1.4	-4.4	-4.1	-3.9
80	81	80.1	79.9	84.4	84.4	92.7	47.5	55.5	57.2
-27.9	32.1	-7.2	10.5	0.8	5.3	4	2.5	-11.8	17.7
1.7	5.4	23.7	24.8	-21.6	-21.6	-11.6	-9.3	-11.8	-8.9
81.5	82.6	88.8	88.5	87.4	87.4	102.1	44.4	52.2	53.3
-23.8	25.3	-8.4	7.8	0.2	4.3	2.9	-1.2	-13.7	12.5
-5.8	-2.9	22.2	22.8	-28.9	-29	-20.7	-11.6	-13.1	-12.3
77	75.3	84.9	82.7	73.3	73.3	88.9	37.7	44.9	43.9
-24.6	27.3	-8.3	9.6	-1.5	0.4	-0.6	1.3	-15.2	16.4
1.7	0.7	22.9	22.9	-23.6	-23.6	-16.6	-11.1	-10.8	-12.4
74.9	73.6	82	81.2	75.5	75.5	88.1	39.6	43.5	41.9
-24.3	27.4	-8.4	9.2	3.1	5.4	4.8	2.8	-9.6	15.8
3.1	6.3	29.8	32.8	-26.5	-26.5	-20.1	-10	-11.9	-10.1
79.8	76.4	85.4	84.6	78.6	78.6	93	39.9	45.9	47
-23.1	23.7	-7.9	6.9	1.1	2.9	2.7	1.3	-10.6	14.7
7.4	7	29.1	27.3	-16.7	-16.7	-11	-4.8	-4.8	-4.8
73.1	72.8	80.5	80.5	75.6	75.6	87.8	37.9	46.5	45.4
-21.4	20.8	-8.3	7	-2.4	1.1	0.7	-2	-14.1	11
9.7	10.9	27.9	28.1	-15.5	-15.5	-7.7	-1.5	-2.7	-2.4
79.2	78.2	85.1	84.7	82.5	82.5	92.3	40.7	48.5	48.4
-26	22.3	-11.7	7.9	-3.1	-0.1	-1.5	-1.5	-14.8	11.8

20.9	22.1	39.7	39	-5.7	-5.7	7.2	4.1	4.6	4.1
80.8	81.5	82.1	85.8	78.1	78.1	90.3	42.7	50.3	49.7
-23.6	25.2	-10.1	9.4	1.5	3.4	2.1	0.2	-11.7	12.6
12.8	14.2	28.2	29.9	-15.2	-15.2	-5.6	-2.2	-2.5	0.2
77.2	76.7	83.1	83.4	75.3	75.3	86.4	42.2	48.8	47.9
-24.9	31.2	-10.2	14.1	3.6	5.2	4	3.5	-11	18.2
1	2	26.1	23.4	-33.9	-33.9	-17.8	-14.6	-13.5	-12.8
85.5	85.7	90.4	91.1	86.9	86.9	98.3	43.7	52.4	53.5
-22.4	24.6	-8	8.5	1.1	3.2	2.9	1.3	-10.6	13.3
2.4	4.2	25.2	27.4	-23.2	-23.2	-17.7	-6.8	-9.3	-8
75.7	75	84.8	84.2	70.9	70.9	86.3	40.2	45.5	45.1
-18	22.8	-6.4	8.6	3.3	6.1	3.8	0.9	-11.9	14
20.8	22.6	48.1	46.7	-6.6	-6.4	8	1.4	3.1	3.5
86.9	83.5	86.5	87.2	91.4	91.1	102.6	48.5	57.6	55.7
-24.1	23.6	-7.2	8.5	0.5	2.9	3.2	-1.3	-14.2	11.9
20.2	18.6	41.2	40.8	-7.5	-7.5	3.9	1.7	2.3	1.7
76.6	75.6	80.5	81.9	81.7	81.7	90.1	41.3	48.4	47.5
-24.6	32	-8	13.5	3.3	5.1	5	3.3	-8.3	16
16.9	20.1	39.5	37	-11.6	-11.6	1.1	1.3	-0.7	-0.5
82.3	83.1	85.1	85	87.3	87.3	98.1	40.9	49.8	52.5
-24.4	21.9	-10.8	8.4	-3.7	-1.3	-2.1	-2.6	-13.7	10.6
23.8	23	46	43.9	-5	-5	8.8	5.1	5.3	4.6
79.1	78.7	68.8	82.1	84.9	84.9	96	43.4	51.2	50.4
-21	30.3	-7.9	10.7	5.6	7.3	7.4	1.5	-11.2	15.9
-0.7	1	25.8	27.3	-23.5	-23.5	-16.8	-8.2	-10.5	-10.5
78.1	75.3	80.2	39.4	76	76	89.3	36.1	44.8	44.4
-26.7	24.9	-10.6	9	-2.2	-0.1	-0.2	-1.2	-14.1	10.8
4	5.6	28.4	31.3	-22.8	-22.8	-14	-8.4	-9.3	-8.2
81.7	79.3	88.2	89	81.4	81.4	94.7	41.4	48.5	48.5
-22.7	28.3	-7.3	11.2	3.1	5.4	4.9	2.4	-9.5	17
0.7	3.8	26.8	27.3	-21.9	-21.8	-11.4	-6.1	-9	-7.2
76.7	76.4	82.6	82.1	74.4	74.4	88.5	37	41.3	42.2
-26.6	29.4	-8.3	9.7	-0.2	2.2	0.4	2.8	-12.5	14.9
11.3	12.4	35.6	33.3	-14	-14	0.4	-6.1	-4.1	-4
81.2	83	86	87.4	90	90	99.8	56.7	55.1	55.8
-20	28	-7.4	11.2	4.9	6.9	6.4	1	-10.5	14.7
5.8	10	32.8	36.9	-20.6	-20.6	-7.8	-6.7	-8.8	-5.7
77.6	75.1	85	85.1	78.4	78.4	93.9	36.8	45.6	44.9
-23	24.7	-8.9	9.4	-0.5	1	1.1	-0.3	-13.1	13.2
13.1	15.6	41.2	40.3	-13.9	-13.9	-0.9	-2	-3.8	-4.1
79.1	80.3	83.8	84.5	84.4	84.4	99.8	39.4	49.2	48.4

-24.9	26.8	-9.9	11.4	0.2	2.7	1.7	-0.3	-13.7	13.9
15.7	17.2	39.9	39	-5.9	-5.9	4.5	-0.5	-0.6	-0.3
84.7	82.8	84.5	84.4	89	89	98.6	47.3	55.8	56.3
-24.2	26.3	-8.7	7.5	2.2	3.9	3.1	0.1	-11.1	16
15.7	18.4	40.8	41.3	-9.7	-9.7	-2.8	-4.6	-4.1	-2
83.5	85	90.5	90.9	86.2	86.2	102.2	48.1	51.8	55.2
-25.5	20.2	-11.2	6.3	-5.6	-4.1	-2.7	-4.8	-18.3	8.8
14.6	11.7	33.9	33.8	-12.4	-12.4	-4.1	-1.2	-0.9	-3.3
77.6	75	81.4	81.4	78.6	78.6	87.1	42.9	48.1	45.1
-24.1	23	-9.6	9	-3.3	-0.1	-1.1	0.3	-12.6	11.4
5.5	6.3	28.9	27.8	-18.3	-18.3	-7.9	-4.1	-4.2	-3.8
74.2	77.3	81.5	82.2	77.9	77.9	90	40.6	48.9	48.5
-22.2	20.6	-7.6	7.4	-2.9	-1.1	-1.9	0.2	-11.9	11.7
5.5	4.2	31.8	31.1	-18.5	-18.5	-11.8	-0.3	-3.4	-1.7
80.9	82.2	88.4	89.5	83.3	83.3	95.7	43.4	51.4	51.4
-29.4	22.5	-11.8	7.1	-5.6	-1.7	-3.7	-2.6	-16.7	12
5.8	5.9	28.5	28.1	-15.8	-15.7	-13.2	-6.3	-7.8	-7
79.8	81.8	84.6	86.1	84.9	84.9	95.4	44.7	50.1	51
-27	27.1	-8.6	8.8	-1.5	1.3	-0.1	0.9	-12.7	15.2
8.1	9.4	35	32.1	-15.7	-15.7	-6.3	-3.3	-2.4	-3.1
75.9	77	82.2	82.5	79.5	79.5	86.6	39.9	46.7	46.7
-26.7	21.7	-9.7	6.3	-2.7	-0.3	-1.9	-1.9	-15.1	9.8
12.3	15.3	33.8	37.9	-9.1	-9.1	-1.1	-0.5	-0.5	1.3
75.1	74.3	78.9	77.1	76.5	76.5	87.5	42	47.6	47.3
-26	27.4	-10.6	11.2	1.1	5.1	3.7	2.2	-11.6	16.4
25.3	26.1	46.5	45.3	-3.1	-3.1	9.4	3	4.3	4.9
81	82.3	82.1	84.6	88.5	88.5	98.6	46.2	51.7	52

Reliability data.

IOR	-28.1	-1.2	78.3	IOR	-28.1	0.8	78.9
IOL	31	2.6	80.4	IOL	31	4.6	80.9
LDR	-7.3	21	87.1	LDR	-7.3	23.1	87.4
LDL	10.1	20.6	87.5	LDL	10.1	22.6	87.8
NPFR	0.8	-21.9	84.4	NPFR	0.8	-19.9	85.3
NPFL	5	-21.9	84.4	NPFL	5	-19.9	85.3
ANS	1.5	-13.7	98.2	ANS	1.5	-11.5	98.9
PNS	3	-8.7	43.7	PNS	3	-7.2	44.4
GPFR	-10.7	-12.5	50.5	GPFR	-10.7	-10.9	51.2
GPFL	17.6	-9.3	52.2	GPFL	17.6	-7.7	52.9

IOR	-24.9	2.7	74.8	IOR	-24.3	1.3	73.7
IOL	25.9	2	72.4	IOL	27.1	1.1	72
LDR	-8.7	22.3	81	LDR	-7.3	25.1	80.5
LDL	9.4	23.1	80.2	LDL	9.8	25.9	79
NPFR	-1.8	-21.4	75.1	NPFR	0.1	-22.1	74.6
NPFL	1.3	-21.4	75.1	NPFL	2.4	-22.1	74.6
ANS	0.4	-12.7	88.4	ANS	-0.1	-14.8	85.7
PNS	-0.1	-10	39.9	PNS	1.4	-9.6	39.6
GPFR	-15.1	-10	45.3	GPFR	-13.8	-11.1	44.5
GPFL	14.7	-10.7	43.3	GPFL	16	-11.7	43

IOR	-22.4	8.6	73	IOR	-22.7	10	72.3
IOL	23.3	7.3	73.2	IOL	22.4	8.3	73.3
LDR	-7.5	29.2	80.7	LDR	-7.8	29.9	80.3
LDL	7.7	27.4	80.3	LDL	7.6	28.1	80.4
NPFR	0.5	-16	75.7	NPFR	-0.1	-15.1	76.2
NPFL	2.3	-16	75.7	NPFL	1.9	-15.1	76.2
ANS	0.1	-9.2	87.2	ANS	0.9	-8.2	86.1
PNS	2	-3.4	39.6	PNS	2.2	-2.6	39.3
GPFR	-10.2	-3.3	47.6	GPFR	-10.1	-2.4	47.3
GPFL	14.3	-3.7	46.2	GPFL	14.5	-2.7	46.7

IOR	-23.4	17.1	83.6	IOR	-24.3	20.3	78.7
IOL	23.6	21.3	79.7	IOL	22.6	22.2	80.2
LDR	-8.7	42	84.9	LDR	-9.6	46.5	82.6
LDL	8.5	42.3	84.9	LDL	7.5	46.2	84.9
NPFR	0	-6	77.1	NPFR	-1.7	-4.3	76.3
NPFL	3.3	-6	77.1	NPFL	1.9	-4.3	76.3
ANS	1.9	6.3	89.4	ANS	-0.1	7.9	88.6
PNS	-2.2	2.4	43.4	PNS	0.4	4	41.9
GPFR	-13.9	2.8	50.6	GPFR	-12.3	5.2	47.9
GPFL	12.1	4	49.5	GPFL	14.6	5.8	49.5

IOR	-24.4	6.7	83.3	IOR	-24.7	6.1	82.1
IOL	30	6.9	83.5	IOL	30	6.8	82.6
LDR	-10.7	34.5	84.4	LDR	-10.8	35.1	83.9
LDL	13.3	36.2	85.6	LDL	13.4	37	83.8
NPFR	1.8	-27.1	86.3	NPFR	1.9	-26.8	85.4
NPFL	3.4	-27.1	86.3	NPFL	3.9	-26.8	85.4
ANS	2.9	-10.6	96.9	ANS	3	-10.8	94.7
PNS	2.4	-9.5	43.5	PNS	2.1	-9.8	43.2
GPFR	-9.3	-11	52	GPFR	-10.9	-8.9	50.6
GPFL	15.3	-11	53.9	GPFL	16.6	-8.2	51.8

IOR	-18.4	17.8	86.5	IOR	-18.5	17.8	85.5
IOL	20.7	19.4	83.4	IOL	21.6	20	83.3
LDR	-9.1	36.8	89	LDR	-8.9	37.6	88.3
LDL	7	44.9	87.3	LDL	7.4	43.8	88
NPFR	1.5	-8.1	88.5	NPFR	2	-7.2	89.1
NPFL	4.5	-8.1	88.5	NPFL	4.7	-7.2	89.1
ANS	0.7	6.3	101.2	ANS	1.7	6.2	100.3
PNS	-0.3	0.6	47.9	PNS	1.2	1.1	49.2
GPFR	-11.7	1.5	57.8	GPFR	-11.2	2.1	57.1
GPFL	11.4	1.6	56.4	GPFL	13	2.6	56.7

IOR	-23.9	17	82.8	IOR	-24	16.9	82.4
IOL	32.1	21.9	82.3	IOL	32.3	20.9	82.3
LDR	-7.1	42.2	84.8	LDR	-7.5	43.1	84.1
LDL	11.7	42.3	84.6	LDL	11.4	42.8	84.4
NPFR	5.1	-9.5	87.2	NPFR	4.7	-10.3	87.3
NPFL	6.8	-9.6	87.2	NPFL	6.6	-10.3	87.3
ANS	6.3	2.8	98.1	ANS	6	2.1	96.9
PNS	3	1.8	42.3	PNS	4.1	1.1	42.4
GPFR	-8.1	0.7	49.7	GPFR	-7.6	0	49.6
GPFL	15.9	1	51.9	GPFL	16.1	0.2	51.9

IOR	-26.2	4.9	81.4	IOR	-27.1	5.9	81.1
IOL	25.2	7.8	77.7	IOL	25.3	8.5	77.1
LDR	-10.3	29.6	88.1	LDR	-10.2	30.9	88.7
LDL	9.3	33.7	87.6	LDL	9.2	33.7	86.7
NPFR	-1.5	-21.2	81.7	NPFR	-1.9	-20.4	81.6
NPFL	0.5	-21.2	81.7	NPFL	0.9	-20.4	81.6
ANS	-0.2	-12.1	94.7	ANS	-0.1	-11.7	92.7
PNS	-0.6	-7.4	43	PNS	-1.1	-7.2	43.4
GPFR	-14.1	-8.1	48.9	GPFR	-14.6	-7.6	49
GPFL	11	-7.1	48.5	GPFL	10.8	-6.4	48.3

IOR	-23.3	15.2	81.2	IOR	-24.4	14.7	80.4
IOL	25.7	17.3	83.6	IOL	29	16.5	80.4
LDR	-9.1	40	88.7	LDR	-9.5	39.3	87.7
LDL	8.1	41.3	88.6	LDL	7.7	40.3	88.3
NPFR	0.7	-10	84.5	NPFR	-0.5	-10.3	83.6
NPFL	2.8	-10	84.5	NPFL	2.8	-10.3	83.6
ANS	0.4	-1.7	97.7	ANS	2	-2.4	96.3
PNS	2.8	-3.5	47.3	PNS	2.8	-3.1	47.3
GPFR	-10.5	-3.4	50.6	GPFR	-11.2	-4	50.3
GPFL	17.3	-1.6	50.7	GPFL	16.4	-2.3	50.8

IOR	-24	14.6	73.9	IOR	-25	15	73.5
IOL	20.9	13.3	72.2	IOL	20.3	12.3	71.6
LDR	-10.8	33.5	77.7	LDR	-11.4	33.6	77.5
LDL	6.6	33.3	78.3	LDL	6.2	33.4	78.2
NPFR	-4.2	-11.4	75.3	NPFR	-5.4	-11.8	74.2
NPFL	-2.1	-11.4	75.3	NPFL	-3.7	-11.8	74.2
ANS	-0.5	-2.8	84.4	ANS	-1.5	-2.7	82.6
PNS	-2.4	0.2	39.7	PNS	-3.4	0.4	39.5
GPFR	-15.8	-0.7	45.8	GPFR	-17.4	-0.6	45.4
GPFL	10.3	-1.5	44.4	GPFL	9.7	-2	42.6

IOR	-23.9	3.5	75.1	IOR	-24.8	5.3	73.7
IOL	23.2	4.8	77.4	IOL	23.3	6	77.1
LDR	-9.6	29.3	82.9	LDR	-9.7	31.1	81.6
LDL	9.2	25.9	82.7	LDL	9	27.5	82
NPFR	-2.2	-19.1	77.6	NPFR	-3.2	-18.1	77.8
NPFL	0.1	-19.1	77.6	NPFL	0	-18.1	77.8
ANS	-0.6	-10.5	90.1	ANS	-0.8	-8.9	89.2
PNS	-0.6	-6.2	42.5	PNS	-0.4	-5.1	42.5
GPFR	-12.7	-6	49.5	GPFR	-12.5	-4.7	48.8
GPFL	11.8	-4.9	49	GPFL	12.6	-3.6	48.4

IOR	-23.7	12.7	80.2	IOR	-23.9	13.9	79.2
IOL	24.9	12.6	81	IOL	23.7	12.4	79.2
LDR	-8.9	36.9	79.4	LDR	-9.2	37.3	78.7
LDL	10.8	37.7	79.5	LDL	10.6	37.5	78.2
NPFR	-1	-6.5	85	NPFR	-2.3	-5.6	82.9
NPFL	1.7	-6.5	85	NPFL	0.7	-5.5	82.9
ANS	0.3	2.1	92.9	ANS	-0.9	2.8	90.4
PNS	0	-4.3	47.9	PNS	-1.4	-3.1	48.2
GPFR	-11.9	-3.2	53.7	GPFR	-13.7	-1.9	54.9
GPFL	13.6	-3.7	54.7	GPFL	11.8	-3.3	51.9

IOR	-23.5	2.2	79.2	IOR	-24.5	4.5	78.6
IOL	19.3	-0.1	79.4	IOL	19.2	2.1	79.3
LDR	-7.4	28.4	88.7	LDR	-8.2	30.8	87.5
LDL	7.7	27.5	88.9	LDL	7.5	29.7	88.2
NPFR	-4.1	-20.9	79.8	NPFR	-4.8	-18.4	80.4
NPFL	-2.2	-21	79.8	NPFL	-3.1	-18.4	80.4
ANS	-2.9	-14.1	92.9	ANS	-4.4	-11.3	93.2
PNS	-1.6	-1.5	41.2	PNS	-1.7	-0.1	41.6
GPFR	-13.6	-4.1	50.4	GPFR	-13.9	-2.4	50.7
GPFL	9.7	-3.4	49.4	GPFL	9.4	-1.4	49.6

IOR	-24.8	7.2	73.2	IOR	-26.1	8.2	73
IOL	26.9	9.8	73.8	IOL	25.8	9.5	75.2
LDR	-8.4	33.6	80.7	LDR	-8.7	34.1	80.1
LDL	8.4	33.3	80.4	LDL	7.5	34.1	80.7
NPFR	0.1	-15	76.5	NPFR	-1.5	-14.2	76.8
NPFL	3	-15	76.5	NPFL	1.8	-14.3	76.8
ANS	1.4	-6.2	85.8	ANS	0.9	-5.7	85.8
PNS	0.9	-3	38.2	PNS	1	-2.4	38.6
GPFR	-11.9	-2.7	45	GPFR	-12	-2.1	45.2
GPFL	14.7	-2.5	44.8	GPFL	14.7	-2	45.1

IOR	-24.3	21.1	80.7	IOR	-25.5	22.1	79.8
IOL	22.6	21.8	82.5	IOL	22.2	23.1	81.9
LDR	-12.2	38.3	83.1	LDR	-12.4	39.6	84.3
LDL	8.7	37.8	86.7	LDL	7.8	41.5	85.6
NPFR	-2.7	-5.7	78.3	NPFR	-2.9	-4.6	78.1
NPFL	1.3	-5.7	78.3	NPFL	0.3	-4.6	78.1
ANS	-0.9	7	90.5	ANS	-1.6	8.5	89.4
PNS	0	4.1	43.2	PNS	-1.1	4.2	42.9
GPFR	-13.2	4.8	50.1	GPFR	-14	5.6	48.7
GPFL	13.5	4.8	50.5	GPFL	12.6	5.2	49

IOR	-18.5	19.4	86.9	IOR	-20.7	20.4	85.8
IOL	23	20.6	83.3	IOL	20.8	20.6	84
LDR	-6.1	46.6	87.6	LDR	-7.1	47.8	87.5
LDL	8.8	43.7	88.3	LDL	6.9	46.3	87.6
NPFR	3	-8.3	91	NPFR	-0.1	-7.8	90.7
NPFL	6	-8.3	90.9	NPFL	3.2	-7.9	90.7
ANS	2.8	6.4	103	ANS	1	6.6	102.1
PNS	0.6	0.3	48	PNS	-0.1	1.1	48.2
GPFR	-11.1	1.4	57	GPFR	-13.3	2.6	57.1
GPFL	13.7	1.7	54.6	GPFL	12.4	2.2	55.7

IOR	-20.7	-0.7	78.3	IOR	-22.1	-0.6	77.8
IOL	30.4	1.3	75.4	IOL	29.8	0.6	75.4
LDR	-8.2	26.2	80	LDR	-8.1	25.6	81.1
LDL	10	27.2	81.5	LDL	9.7	26.7	82.5
NPFR	5.9	-23.6	76.1	NPFR	4.3	-22.8	76.1
NPFL	7.5	-23.6	76.1	NPFL	6.7	-22.8	76.1
ANS	7.3	-16.3	89.6	ANS	6.2	-16.1	89.1
PNS	1.3	-8.6	36.4	PNS	0.6	-8.1	36.8
GPFR	-11.6	-10.1	44.5	GPFR	-12.3	-9.9	44.5
GPFL	16.1	-10.1	44.2	GPFL	15	-10.3	44.1

IOR	-22	13	78.8	IOR	-23.3	13.5	78.8
IOL	24	14.7	80.5	IOL	24.3	14.9	80.8
LDR	-8.8	40.6	83.8	LDR	-10.2	35.3	84.8
LDL	9	39.8	84.8	LDL	9.7	39	84.7
NPFR	-1.1	-14.3	84	NPFR	-0.8	-14.4	84.2
NPFL	0.7	-14.3	84	NPFL	0.9	-14.5	84.2
ANS	0.2	-1.4	99.9	ANS	0.4	0.1	94.3
PNS	0.2	-2	39.3	PNS	0.6	-2	39.5
GPFR	-12.8	-4	50.2	GPFR	-13.3	-3.6	50.3
GPFL	14	-4.2	49.8	GPFL	14.7	-4.3	49.8

IOR	-25.5	15.5	82.4	IOR	-23.9	17.2	82.1
IOL	25.6	17.3	83.9	IOL	26.6	19	83.2
LDR	-9.2	38.6	90.1	LDR	-8.3	42	89.1
LDL	8	39.4	89.8	LDL	8.2	42.2	88.9
NPFR	1.2	-10.3	85.3	NPFR	2.2	-8.4	85.3
NPFL	2.7	-10.3	85.3	NPFL	3.8	-8.5	85.3
ANS	1.5	-3.4	100.9	ANS	3.4	-0.8	100
PNS	1	-4.7	48.3	PNS	2.3	-2.6	48.2
GPFR	-12.1	-4.5	52	GPFR	-11.5	-3.3	51.4
GPFL	17.3	-3.2	48.4	GPFL	17.4	-1.4	48

IOR	-29.4	6.2	80.3	IOR	-30.1	7.3	79.7
IOL	22.1	6.4	81.9	IOL	21.8	6.2	81.7
LDR	-12.2	28.2	84.7	LDR	-12.3	29.5	85.5
LDL	7.2	28.8	86.5	LDL	6.9	29.4	86.2
NPFR	-5.9	-15.9	85	NPFR	-6.7	-15.5	85.3
NPFL	-2.2	-15.9	85	NPFL	-3.1	-15.5	85.3
ANS	-3.8	-12.5	94	ANS	-4.7	-11.4	94
PNS	-2.8	-6.7	44.6	PNS	-2.9	-6	44.9
GPFR	-17.4	-7.7	50.6	GPFR	-17.6	-7.2	50.3
GPFL	11.6	-7.1	51.2	GPFL	10.8	-7.1	50.7

Average Coordinates			SD of Averages Coordinates		
-24.00	10.58	79.39	2.54	7.01	4.06
25.00	11.63	79.35	3.60	7.48	4.00
-9.13	34.34	84.21	1.53	7.04	3.65
8.88	34.77	84.54	1.72	7.39	3.63
-0.46	-14.32	81.74	2.89	6.62	5.09
2.15	-14.33	81.73	2.77	6.63	5.08
0.93	-4.55	93.49	2.62	7.96	5.56
0.38	-3.23	43.06	1.77	4.14	3.69
-12.52	-3.63	49.92	2.16	4.89	3.64
13.85	-3.17	49.71	2.32	4.65	3.84

SD of all x3		
2.57	8.14	8.98
3.61	7.43	8.48
1.56	8.87	6.55
1.73	8.01	6.53
2.94	6.71	12.38
2.80	6.84	12.38
2.68	7.77	12.54
1.84	4.04	6.39
2.21	4.94	7.07
2.38	4.93	7.08

Total Av. ABC		(differences between reliability recordings)	Average	(of all 3 reliability recordings)	
0.75	0.84	0.81	0.57	0.61	0.69
0.71	0.74	0.76	0.46	0.68	0.68
0.45	1.28	0.79	0.36	0.85	0.62
0.44	1.30	0.67	0.45	1.19	0.67
0.87	0.80	0.51	0.61	0.62	0.44
0.77	0.80	0.50	0.67	0.63	0.42
0.86	0.94	1.22	0.89	0.69	0.59
0.82	0.64	0.47	0.77	0.56	0.57
0.79	0.72	0.64	0.77	0.60	0.64
0.87	0.76	1.02	0.83	0.78	1.14